6. Telescope Performance

This chapter presents the expected performance of the KM3NeT neutrino telescope. Detailed detector simulations have been performed, and expected neutrino rates from some example astrophysical sources estimated. From these, in particular, the sensitivity to point sources (assuming a pure E^{-2} neutrino spectrum) has been computed.

Given that as yet no observations of high energy neutrinos from extra-terrestrial sources have been made, these rate estimates must rely on models of neutrino production in the sources. These estimates have significant uncertainties, the magnitude of which depends on the nature of the source.

In many models of production of high energy astrophysical radiation, charged particles are accelerated in shock waves and neutrinos are produced in interactions of these accelerated particles with matter or radiation fields in the vicinity of the source. A typical reaction is $pp \rightarrow \pi + X$, followed by the decay of the charged pions $\pi \rightarrow \mu\nu_\mu$. In the same reaction, gamma rays are produced in the decay of neutral pions $\pi^0 \rightarrow \gamma\,\gamma$ and so a link can be made between the neutrino and gamma production rates. In general, many final states contribute to the full neutrino rate and detailed predictions must be based on Monte-Carlo simulations of the interactions [46,47]. Pion production and decay are well understood from particle physics. Uncertainties arise from using approximations and simplified parametric approaches and from considering incomplete sets of neutrino production channels. Furthermore, in dense source environments multiple interactions are important and the rate of particle decay compared to further interaction must be taken into account. In some models of dense sources [48], e.g. in the case of gamma ray bursts, the high-energy neutrinos are dominantly produced from kaon decays rather than pion decay because of the shorter meson lifetime.

For sources with low matter density, where secondary particle absorption is small, a fairly reliable neutrino rate prediction can be made based on the observed gamma fluxes. This class of sources includes supernova remnants such as RX J1713.7-3946 and RX J0852.0-4622 which are observed in gamma rays as extended objects with angular sizes of 1-2°. For compact objects such as microquasars, absorption of gammas could be important and so neutrino rate predictions must be based on modelling of the corresponding processes. For even denser environments, in particular observed GRBs and the hypothesised "failed GRBs", the predictions are very uncertain.

For the event rate predictions presented in this chapter, the uncertainty of the assumed neutrino fluxes from supernova remnants can be estimated to be roughly a factor of 2. For other sources the predictions must be taken as order-of-magnitude estimates.

6.1 Analysis Techniques

In this section the techniques are presented to identify event candidates in the data, reconstruct them, suppress background and search for signals of cosmic neutrinos.

6.1.1 Background Suppression

There are two different kinds of background related to high-energy particles: atmospheric muons and atmospheric neutrinos. Both are produced by the interaction of primary cosmic rays with the atmosphere. The flux of atmospheric muons at sea surface exceeds that of neutrino-induced muons in the detector by about 10 orders of magnitude. These muons, however, are attenuated in flux and energy below sea surface as a function of depth and zenith angle. Their flux falls to zero near and below the horizon where they are stopped by the water and earth shielding. For this reason astrophysical neutrino signals are mainly searched for among muons from the downward hemisphere. Accurate reconstruction procedures and quality cuts on reconstructed tracks are needed to eliminate atmospheric muon tracks that are mis-reconstructed as up-going.

Atmospheric neutrinos traverse the Earth and are detected in the same way as signal neutrinos. They are thus an unavoidable source of background and must be discriminated from the signal in the data analysis with energy cuts and on statistical grounds.
For atmospheric neutrino simulation, the Bartol flux [49] was used. A prompt contribution from charm decays is included according to the highest prediction of the Recombination Quark Parton Model [50]. The atmospheric neutrino flux has an energy spectrum approximately proportional to $E^{-3.7}$ and an isotropic distribution, while neutrinos from astrophysical point sources point to their origin and are expected to follow an energy spectrum close to E^{-2}. Applying a search cone around the source position with a width reflecting the angular resolution of the detector and energy cuts are thus the prime methods to increase the signal-to-background ratio for point source searches.
A different source of background is the optical noise in sea water that superimposes random hits that are not correlated to the neutrino signal. This background is due to the presence of radioactive isotopes (mainly ^{40}K) and bioluminescent organisms (see Sections 5.2.5 and 5 2.6). The uncorrelated background produced by ^{40}K decay is about 40 kHz for 8-inch PMTs (at a threshold of 0.3 photoelectrons). Bioluminescent bacteria may produce an additional slowly varying background level. To cope with the optical backgrounds, specific online data filter procedures and offline hit selections are applied.
Larger bioluminescent organisms (from plankton to fish) produce bursts of light that saturate close-by PMTs which are then excluded from the data analysis.

6.1.2 Online Data Filter

The data stream to shore contains information of all PMT signals above a given threshold. Online filters based on high amplitude and coincident signals on adjacent PMTs are applied to select candidate events from this stream, which are then stored for further analysis (see Section 3.2). For the sensitivity studies presented here, no simulation of this online filter was necessary since the quality and selection cuts applied at later analysis stages are much more selective than the filter criteria.

6.1.3 Muon Reconstruction

The central challenge in measuring muon neutrinos is the reconstruction of the muon trajectory from the PMT signals. For an assumed muon trajectory the expected arrival times of the Cherenkov photons at the optical modules are calculated, using the geometrical positions of the PMTs, the group velocity of light in water and the Cherenkov angle of about 43°.
Time residuals are determined as the differences between the expected and the measured arrival time of the photon(s) on a given PMT. Photons that scatter in the water and photons emitted by secondary particles lead to residuals with increased magnitude. The reconstruction algorithms aim at finding muon track parameters for which the residuals are small in magnitude. This is done by maximising the sum over PMTs of a "score function" that is designed to be large when the residuals are small. In the final stage of the algorithm, the score function is the logarithm of the probability (log-likelihood) of a residual.
The background light from ^{40}K and bioluminescence potentially degrades both the angular resolution and the reconstruction efficiency. The algorithm accounts for this background by incorporating it into the probability function. A full description can be found in [51].
The probability density function of the arrival time residuals has been derived from simulations with the ANTARES software. It takes into account the probability of photons arriving late due to scattering or emission from secondary particles. Moreover, the probability of a hit being due to background is accounted for as a function of the hit amplitude. The overall log-likelihood value per degree of freedom obtained from the final fit is used as a measure of the fit quality.
The contribution of the background hits results in a likelihood function that has many local maxima as a function of the track parameters. As a consequence, the fit only converges to the correct solution if the start values are already a good approximation to this solution. The final likelihood fit is therefore preceded by a series of prefit algorithms of increasing sophistication.

The score functions used in these prefits are designed to yield an adequate trade-off between an accurate description of the true hit residuals and high efficiency for finding the global maximum. They allow for convergence to a solution which is typically within a few degrees of the true muon direction, while being robust against the presence of background hits with large residuals. Since not all parameters and probability density functions used in the muon reconstruction could as yet be optimised to KM3NeT in its different design options, there is room for further improvement of reconstruction efficiency and precision. For example, it has recently been demonstrated that an increase of the reconstruction efficiency in KM3NeT is achievable by replacing the prefits by a scan of the trajectory parameter space to define appropriate starting points for the final track optimisation. An alternative reconstruction algorithm is used in the SeaTray framework described in Section 6.2.2. This algorithm uses the Pandel parameterisation of the time residual distribution [52,53,54], which is a function derived from the physics laws of the underlying processes, with three free parameters determined from Monte Carlo simulations for various distances from point light sources. Despite the fact that it only has a small number of free parameters, it can accurately parameterise a large range light transmission phenomena. It is for this reason that it can also be used for muon tracks, which in principle have a light emission profile different from point sources of light.

6.1.4 Sensitivity Calculation

The number of detectable events from a neutrino source is related to the neutrino flux and to the detector response by the following relation:

$$N_s = \iint A^{\nu}_{eff}(E_\nu, \theta_\nu) \frac{d\Phi_\nu}{dE_\nu d\theta_\nu} \, dE_\nu \, d\theta_\nu$$

In this definition, $\frac{d\Phi_\nu}{dE_\nu d\theta_\nu}$ is the predicted astrophysical neutrino flux, E_ν is the neutrino energy and θ_ν is the neutrino angle with respect to the detector coordinate system. The neutrino effective area A^{ν}_{eff} is given by:

$$A^{\nu}_{eff}(E_\nu, \theta_\nu) = V_{eff}(E_\nu, \theta_\nu) \times \rho N_A \times \sigma(E_\nu) \times P_{earth}(E_\nu, \theta_\nu) \,,$$

where ρN_A is the number of nucleons per unit volume (ρ is the effective matter density in mol per volume and N_A the Avogadro number), $\sigma(E_\nu)$ is the neutrino cross section in the reaction channel considered, and P_{earth} is the neutrino transmission probability through the Earth. The quantity $V_{eff}(E_\nu, \theta_\nu)$ is the detector effective volume which is evaluated from the ratio between the numbers N_{rec} of reconstructed events and N_{gen} of neutrino interactions inside a generation volume V_{gen}, generously encompassing the instrumented volume. The effective volume is then given by:

$$V_{eff}(E_\nu, \theta_\nu) = \frac{N_{rec}(E_\nu, \theta_\nu)}{N_{gen}(E_\nu, \theta_\nu)} V_{gen}$$

The search for cosmic neutrino signals is based on statistical techniques that are appropriate for the detection of small numbers of events. The discovery potential of the neutrino telescope is evaluated using the model discovery potential (MDP) [52] calculated for a given level of significance ($3\sigma, 5\sigma, \ldots$) and probability to make a discovery (70%, 90%, ...). In this case cuts are optimised in order to obtain the least signal necessary to claim a discovery.

When no significant signal is observable, limits are set using the model rejection factor (MRF) [55]. In this case, the cuts are optimised to obtain the lowest possible expected upper limit for the experiment, assuming that no true signal is present. The average flux limit that can be placed on a neutrino flux model is defined by

$$\Phi_{90} = \Phi_S \cdot MRF = \Phi_S \frac{\bar{\mu}_{90}(\langle N_{bkg} \rangle)}{\langle N_s \rangle} \,,$$

where Φ_S is the normalisation factor of the flux model. The MRF is defined as the ratio between the average upper experimental limit $\bar{\mu}_{90}$ on the number of signal events and the expected average number of signal events from the source for given Φ_S. The parameter $\bar{\mu_{90}}$ depends on the mean number of background events and is calculated following the Feldman-Cousins approach [56]. The sensitivity values reported in this document are obtained by minimising the Model Rejection Factor, unless explicitly stated otherwise.

6.2 Simulation

This section describes the software packages used for the Monte Carlo simulation. These packages generate neutrinos from astrophysical sources as well as atmospheric muons and atmospheric neutrinos. The code simulates the particle interactions with the medium surrounding the detector, light generation and propagation as well as the detector response.
Two principal and two alternative simulation chains have been used during the Design Study. The results presented in this chapter are produced by the two principal chains, one based on the ANTARES software and the other, named SeaTray, based on the IceCube software framework. Cross- checks on results have been made using these two chains and with the two alternative codes.
In all simulation chains a volume surrounding the instrumented volume, called "can", is defined. The can volume is a cylinder with height and radius exceeding the instrumented volume by about 3 absorption lengths. In the can volume, muons, taus and electrons are propagated and the Cherenkov light is generated.

6.2.1 ANTARES Software

Neutrino and anti-neutrino induced events are generated with the code GENHEN. Within GENHEN, neutrinos of all flavours with energies up to about 10^9 GeV are propagated through the Earth and their interactions simulated. Both charged current (CC) and neutral current (NC) reactions are implemented. The deep-inelastic scattering is simulated with the LEPTO code [57]. The quasi-elastic scattering and resonance production, dominant at low energies, are also taken into account. The propagation of muons and taus in rock or water up to the can surface is performed with MUSIC and TAUSIC [58], respectively.
The background due to down-going atmospheric muons is generated with the code MUPAGE [59] . MUPAGE provides a parameterised description of the underwater flux of atmospheric muons including also multi-muon events. The parameterised muon flux was obtained starting from full simulations with HEMAS [60]and cosmic ray data.
Muons inside the can are tracked with the code KM3 which generates and propagates the light produced by the muons and their secondary particles, taking into account the optical properties of the water. For the photon propagation, the code uses tables containing parameterisations obtained from a full GEANT3 [61] simulation. The code simulates the PMT hit probabilities and the response of the PMTs including the readout electronics. The PMT photocathode area, quantum efficiency and angular acceptance, as well as the transmission of light in the optical module glass sphere and in the optical gel are taken into account.
In order to reproduce the randomly distributed background hits due to optical background (^{40}K and bioluminescence), single photoelectron hits can be added to the muon-induced hits inside a chosen time window. Bursts of bioluminescence, whose effect is to saturate a small number of PMTs over a short period, are estimated to have a negligible effect and are not simulated.

6.2.2 SeaTray

The SeaTray software chain consists of modules organised in the IceTray software framework which has kindly been provided by the IceCube collaboration. The SeaTray package [62] has been specifically developed for use in KM3NeT, both for

the present simulation study and also for the future. SeaTray is a full replacement for the ANTARES software chain presented above and provides the same functionality either using ANTARES packages ported to SeaTray or using alternative modules. In this section only the alternative modules which have been used for the presented results are described.

The propagation through the Earth and the interactions of neutrinos of all flavours are simulated using the ANIS package [63] . Neutrino-nucleon interactions are generated using the CTEQ5 parton distribution functions [64]. CORSIKA [65] is used to generate the atmospheric muon background.

The MMC package [66] performs lepton propagation through matter, which is primarily used to track muons from their point of generation to the detector. The package provides a list of secondary particles above a certain energy threshold produced along the muon trajectory. After a muon has been tracked to and through the detector, light from the muon and its secondary particles is generated and propagated through the detector using the muon-sim[67] package. This package generates Cherenkov photons according to parameterisations produced using a full GEANT4 [68] simulation. Using a set of pre-generated lookup tables, these photons are then tracked through the water taking into account scattering and absorption.

For optical modules with a single PMT, the photons arriving at the optical module are converted into hits using a parameterisation of the angular acceptance. For optical modules containing multiple PMTs, an improved version of this algorithm was developed which performs a simple ray-tracing to identify the PMT that was hit by a particular photon. The PMT readout is simulated with a full time-over-threshold scheme, including a waveform simulation and a time/charge calibration with a time-walk correction. Both reconstruction algorithms described in Section 6.1.3 are implemented in SeaTray.

6.2.3 Alternative Simulations

Beyond the principal simulation chains a fast simulation tool has been developed to compare multiple detector configurations. The software package [69] is a detailed semi-analytic simulation based on the Mathematica software. This flexible tool makes it possible to scan relatively quickly a large parameter space, including design properties (distance between lines and storeys, PMT configurations) and the environmental characteristics (water optical properties, 40K and bioluminescence background). A further complete and independent simulation software [70,71], using GEANT4 for muon propagation and for light simulation, has also been developed. A reconstruction algorithm based on χ^2 minimisation and driven by Kalman filters is part of this package [72]. The results obtained with these alternative packages are in agreement with those of the ANTARES software and the SeaTray framework.

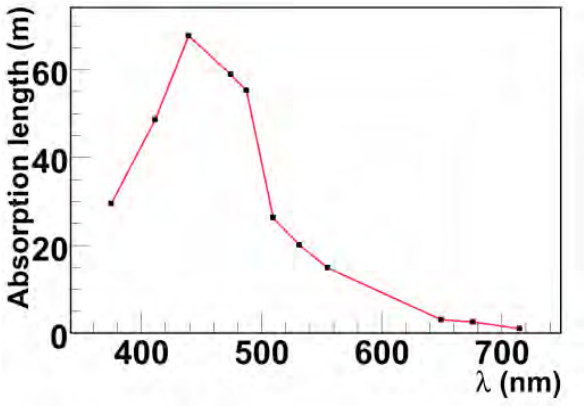

Figure 6-1: Absorption length used in the simulations as a function of wavelength.

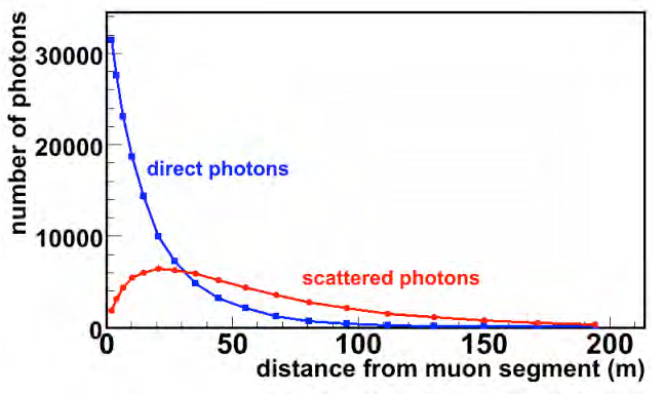

Figure 6-2: Number of Cherenkov photons, from 1 metre of muon path, reaching the given distance from the muon segment.

6.2.4 Sea water properties used in simulations

The simulations are based on the following sea water properties:

- The absorption length, shown in Figure 6-1, corresponds to a measurement at the Capo Passero site, at a depth of 3500m (see Section 5.3 2).
- Light scattering in water has been parameterised according to [73]. This model uses a combination of Rayleigh and Mie scattering, with a relative probability of 0.17 for Rayleigh scattering. The scattering length is computed assuming a concentration of small particles (size < 1μm) of 7.5 per m^3 of water. The same volume concentration is assumed for particles having sizes larger than 1μm.
- The refractive index used for the medium is taken from [74], resulting in 1 35 at 470 nm.

Figure 6-2 shows the number of Cherenkov photons produced per metre of muon trajectory reaching a certain distance. Both absorption and scattering effects are taken into account. This parameterisation is used in the simulation of detected light. Figure 6-3 shows the distribution of time delays induced by the scattering for a given distance to the emission point.

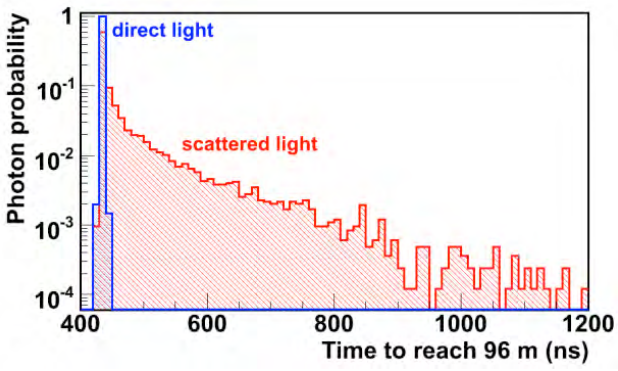

Figure 6-3: Time delay induced by the scattering of light at 96m from the muon segment.

6.3 Sensitivity Studies

The principal scientific objective of the KM3NeT neutrino telescope is neutrino astronomy, targeting the discovery of point-like neutrino sources. Therefore, the telescope optimisation was done with the main focus on such sources, assuming a power-law neutrino energy spectrum proportional to $E^{-\alpha}$ with $\alpha \approx 2$, implying that the main sensitivity must be in the energy range between a few TeV and about one PeV. All three neutrino flavours (ν_e, ν_μ, ν_τ) will be detected in the telescope; however, the best efficiency and angular resolution are achieved for muon neutrino reactions with a muon in the final state. All studies only consider neutrinos coming from below the horizon

For point source searches the MRF method described in Section 6.1.4 is used to evaluate sensitivities. The sensitivities have been obtained applying a "binned" method where the sky is divided in bins of declination and right ascension and the numbers of events detected per bin are analysed. The parameters that are optimised in order to minimise the MRF are the size of the search cone around the source, the cut on the reconstruction quality parameter and a cut on the number of neutrino hits that is related to the neutrino energy. The average number of events from a point-like source, at a given declination and with a spectral index α is estimated by means of Monte Carlo simulations, as well as the average number of background events inside the selected search cone centred on the source direction. The background is due to atmospheric neutrinos and atmospheric muons that are mis-reconstructed as up-going.

6.3.1 Detector Optimization and Performance

Three combinations of technical options as described in Chapter 3 have been investigated in simulation studies:

1. 127 bar-structure detection units arranged in a hexagonal grid (6 m lateral extent, 40 m between storeys, and 180 m between detection units). Each bar is equipped with 3 pairs of 8-inch PMTs.
2. 127 triangle-structure detection units arranged in a hexagonal grid (3 m lateral extent, 40 m between storeys, 150 m between detection units). Each storey is equipped with 3 pairs of 8-inch PMTs arranged in a triangular configuration.
3. 310 string detection units arranged in a rectangular grid (30 m between storeys, 130 m between detection units). Each storey is an optical module equipped with 31 3-inch PMTs.

All these homogeneous configurations are building blocks of the full detector. Detailed optimisation studies have been performed for all options and have led to the choice of dimensions given above. An example of such an optimisation is presented in the following for option 1.

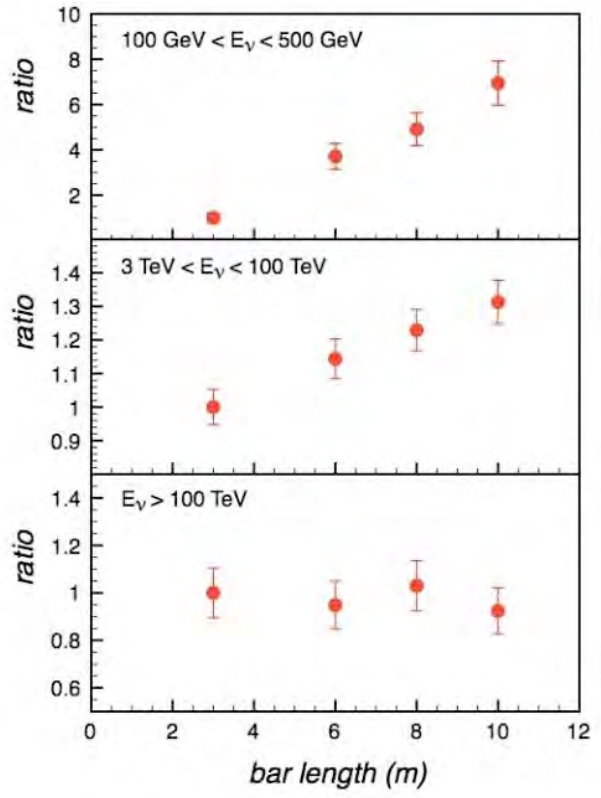

Figure 6-4: The change in neutrino effective area as a function of the bar length for the bar structure detection unit configuration. Shown is the ratio of the effective area relative to a bar length of 3m, for the three energy ranges indicated.

The bar structure offers the advantage that the three-dimensional arrangement of OMs within a single detection unit helps resolve ambiguities in the reconstruction of the azimuthal angle of a muon track. The effect of changing the lateral bar length between 3m and 10m is shown in Figure 6-4. It can be seen that at low and intermediate neutrino energies a significant gain can be obtained for larger lengths. .Taking into account simulation results and technical constraints (such as stability in currents, cost, logistics and safety), a bar length of 6 m is finally chosen as the optimum.

A further example of the optimization is given in Figure 6-5 which shows the point-like source sensitivity as a function of the detection unit separation, which was finally chosen at 180 m, where maximal sensitivity is found [75].

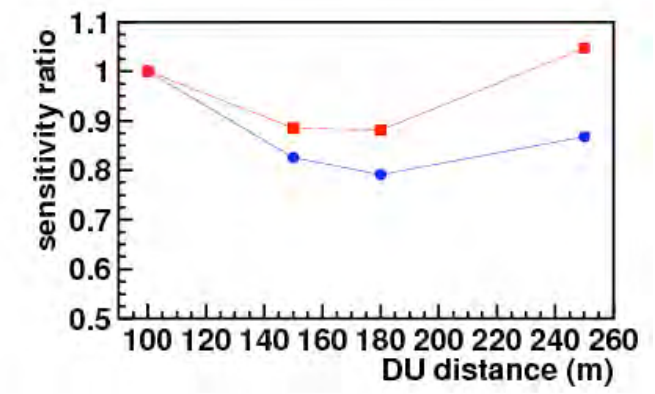

Figure 6-5: Change of the sensitivity of a point source search as a function of the detection unit separations for two different source spectra. The plot shows the ratio of the sensitivity relative to a separation of 100 m. The source spectra are proportional to $E^{-\alpha}$ with blue circles for $\alpha = 2.0$ and red squares for $\alpha = 2.2$.

Figure 6-6 shows the point-source search sensitivity for one year of observation time for one building block of each of the three options mentioned above, as a function of declination.

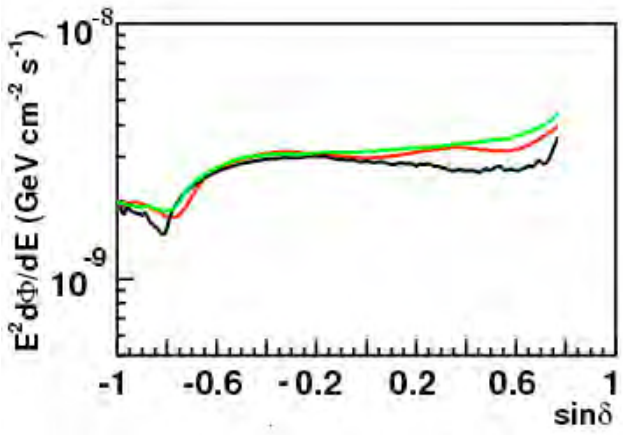

Figure 6-6: Sensitivity to point sources (E^{-2} flux) for one year of observation time, for the three detector configurations studied. The red line is for option 1, the green for option 2 and the black for option 3.

The performances of all building blocks are the same within about 20%. As will be described in Chapter 9 the estimated costs for the three options differ by less than 20%. In Chapter 9, Figure 9-1 shows the sensitivity for a full detector achievable for a capital investment of 220M€ in the three configurations. These final sensitivities are very similar and the best configuration is chosen for all the following results in this document.

The neutrino effective area for this full KM3NeT detector is shown in Figure 6-7 for loose cuts ensuring reasonable angular resolution and for quality cutswhich have been optimised for point-source searches for.

For searches for point-like neutrino sources, the angular resolution is a critical parameter. It is dominated by the intrinsic ν-μ angle at low energies, while at higher energy the telescope response dominates. For a deep-sea neutrino telescope the angular resolution profits from the strongly reduced scattering effects as compared to ice.
The left panel of Figure 6-8 shows the angular resolution, obtained with design option 1, in terms of the angle between the neutrino direction and the reconstructed muon track; in this figure the intrinsic angle between the neutrino and muon directions is also shown.

The cumulative point spread function, after quality cuts, is shown in the right panel of Figure 6-8. The telescope has a superb angular resolution; indeed about 70% of selected events lie within 0.2° of the neutrino direction.

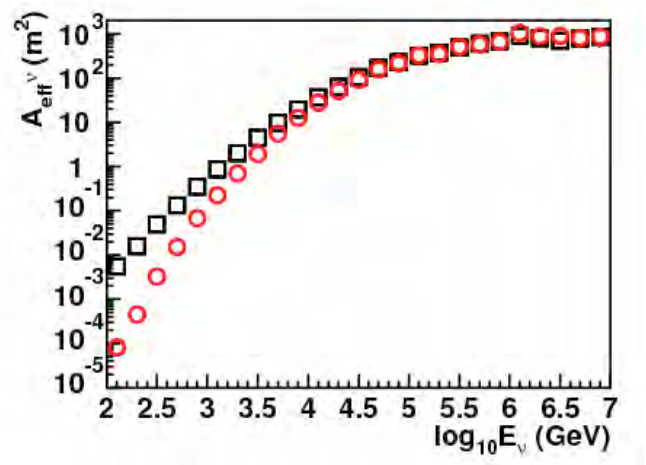

Figure 6-7: Neutrino effective areas for the full detector. The plot is for up-going neutrinos. The red dots are after quality cuts optimised for searches for point-like neutrino sources and the black squares are for looser quality cuts ensuring reasonable angular resolution.

6.3.2 Neutrino Point Sources

The observation of point-like sources of neutrinos would bring unique new insights on the nature of cosmic accelerators and resolve the enigma of the origin of cosmic rays which has been a mystery for the 100 years since their discovery. Observations by gamma ray telescopes have revealed many astrophysical objects, in which high-energy processes at and beyond the TeV level take place (see Figure 6-9); however, measurements with gamma rays alone cannot clearly distinguish whether the accelerated particles are leptons or hadrons. Only the observation of neutrinos from a source can unambiguously establish the hadronic nature of that source. Supernova remnants (SNR) of the shell type are the most probable sources of cosmic rays in the Galaxy. The material ejected during the explosion forms shock waves when it propagates into the interstellar matter. Particles are assumed to be accelerated in these shock waves, which can persist for several thousand years. The shell-type SNRs with the most intense gamma rays fluxes measured beyond 10 TeV are RX J0852.0-4622 (Vela Junior) and RX J1713.7-3946.

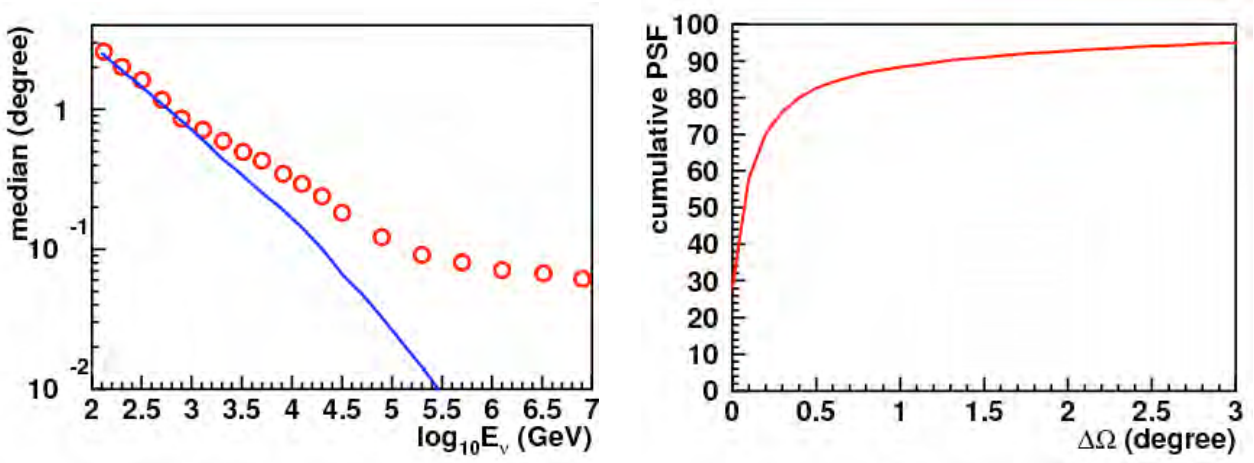

Figure 6-8: Left panel: Median of the distribution of the angle ΔΩ between the neutrino and the reconstructed muon track (red points). The blue line is the median of the intrinsic angle between neutrino and muon directions, driven by the dynamics of deep-inelastic neutrino-nucleon scattering and kinematics. Right panel: Cumulative point spread function for an energy spectrum according to E^{-2}, after quality cuts applied, i.e. the fraction of events with ΔΩ less than a given value.

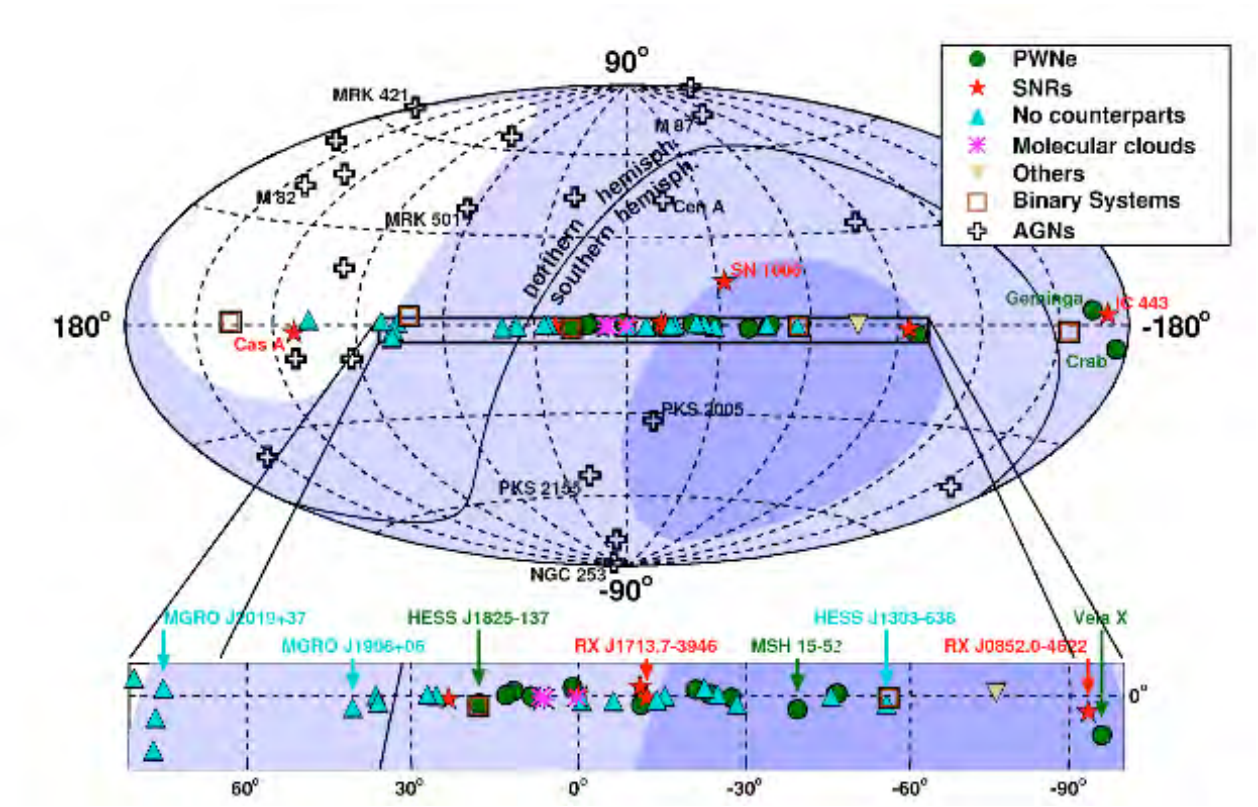

Figure 6-9: Sky coverage in Galactic coordinates for detectors located in the Mediterranean Sea and at the South Pole, where only the northern hemisphere can be observed. The shading indicates the visibility for a detector in the Mediterranean with 2π downward coverage; dark (light) blue areas are visible at least 75% (25%) of the time. The locations of observed sources of high-energy γ rays are also indicated.

Another class of intense gamma sources are the pulsar wind nebulae (PWNe) which differ from the shell-type SNRs in that the acceleration takes place in the region of the central pulsar emitting collimated, very fast-moving material into the surrounding matter. Radio, optical, X-ray and TeV gamma observations suggest a synchrotron origin for these emissions, indicating a leptonic acceleration process. However, for some intense sources such as Vela X, the possibility of a hadronic origin remains valid and they thus could be neutrino sources.

The Galactic Centre region contains many structures which could be neutrino sources, such as the TeV gamma source HESS J1745-290 coincident with the super massive black hole Sagittarius A*, as well as the SNR Sgr A East and the PWN G359.95-0.04. Other potential neutrino sources are microquasars, which are Galactic X-ray binary systems with relativistic jets observed in the radio regime. Among such sources are: GX339-4, SS 433, LS I +61 303 and LS 5039. A major advantage of KM3NeT relative to IceCube is the location in the Mediterranean Sea. Figure 6-9 shows the KM3NeT field of view compared to that of a neutrino telescope at the South Pole. This field of view allows for the observation of up-going neutrinos from a large fraction of the sky (about 3.5 π) including the Galactic Centre and most of the Galactic Plane. In this region many TeV gamma sources have been observed, among them several of those described above as well as further sources that have not yet been identified. It is also noteworthy that the closest extragalactic object in Figure 6-9, the AGN Centaurus A, is located in the southern hemisphere where it is always above the horizon for neutrino telescopes at the South Pole.

The sensitivity of the detector to neutrino point sources, based on one year of data, is shown in Figure 6-10 as a function of the declination. The detector performance is presented as the flux that can be excluded at 90% CL (flux sensitivity) and the flux that can be detected at 5σ with 50% probability (discovery flux). This calculation assumes a neutrino energy spectrum proportional to E^{-2}. For comparison, the plot also shows the flux sensitivity of IceCube [2] (using an unbinned method and a reconstruction algorithm that exploits energy-related information) and the IceCube discovery flux . The latter has been extrapolated from the flux sensitivity using a factor of 2.5 to 3.5 which is based on the corresponding ratio for the IceCube 40-string configuration[76]. The differences in shape of the sensitivity curves for KM3NeT and IceCube are caused by the different geographic location, the effect of neutrino absorption in the Earth and the different detector responses as a function of zenith angle. The use of an unbinned method is expected to give an improvement in the KM3NeT sensitivity of about 40%. From Figure 6-10 it can be seen that the KM3NeT sensitivity is better than that of IceCube over the full range of declinations, even those in the northern sky which is the central field of view from the South Pole. For the southern sky, which is best viewed from the Mediterranean Sea, KM3NeT will have a sensitivity nearly two orders of magnitude better than that of the current instruments, Baikal and ANTARES, whose sensitivity curves fall outside the limits of the figure. To illustrate the importance of this region of the sky, the positions in declination of the Galactic sources indicated in Figure 6-9 are shown.
The sensitivity as a function of the observation time is shown in Figure 6-11.
Many of the Galactic TeV gamma sources shown in Figure 6-9, and in particular the supernova remnants, have an angular size larger than the resolution of the neutrino telescope. For the search for such extended sources a study has been made of the impact of the source size on the sensitivity. Since these sources are in general expected to have a cut-off in their energy spectra at some TeV to some 10 TeV, a neutrino flux proportional to $E^{-2}\exp(-E/20\text{TeV})$ has been assumed. The result of this study, shown in Figure 6-12, indicates that the sensitivity is reduced by a factor of about 2 for typical source diameters of 1°.

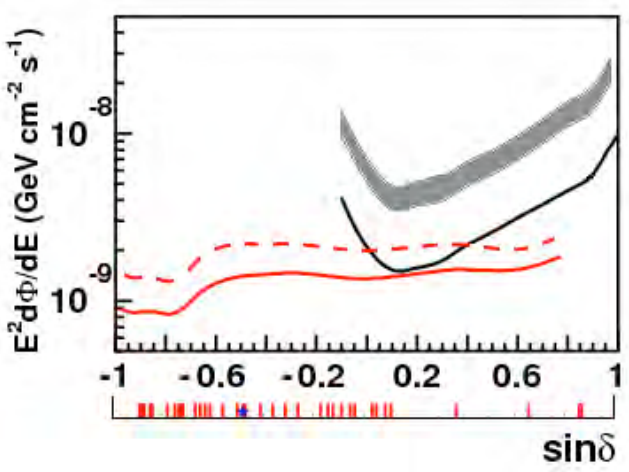

Figure 6-10: Sensitivity of the full KM3NeT detector to neutrino point sources with an E^{-2} spectrum for one year of observation, as a function of the source declination. The red lines indicate the flux sensitivity (90% CL;full line) and the discovery flux(5σ, 50% probability; dashed line). Both are estimated with the binned analysis method. The black line is the IceCube flux sensitivity for one year, estimated with the unbinned method [2] (full line). IceCube's discovery flux (5σ, 50% probability) is also indicated (shaded band, spanning a factor 2.5 to 3.5 above the flux sensitivity). The red ticks at the bottom of the horizontal axis show the positions of Galactic gamma ray sources [3]; the position of the Galactic Centre is indicated by a blue star.

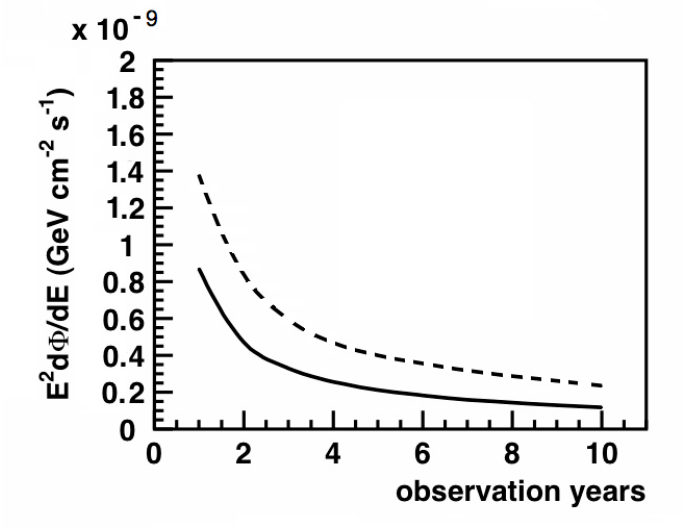

Figure 6-11: Flux sensitivity (90% CL; solid line) and discovery flux (5σ, 50% probability; dashed line) of the full KM3NeT detector as a function of observation time for declination δ =-60° (i.e. sin δ = -0.866) and α =-2.

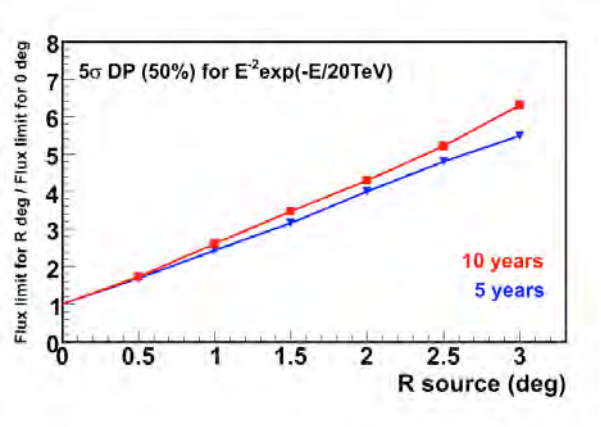

Figure 6-12: Dependence of the discovery flux (5σ, 50% probability) on the angular radius R of a neutrino source. The blue (red) lines and symbols indicate the sensitivities after 5 (10) years of observation, relative to point sources with R=0. For this study, homogeneous emission from the source region and a neutrino spectrum with a cut-off proportional to E^{-2} exp(-E/20TeV) were assumed.

The estimated sensitivity of the detector to neutrino fluxes from these point sources depends strongly on the extension of the spectrum to high energies. Figure 6-13 shows the dependence of flux sensitivity and discovery flux on the assumed cut-off energy. When the cut-off energy decreases from 1 PeV to 10 TeV the sensitivity worsens by an order of magnitude.

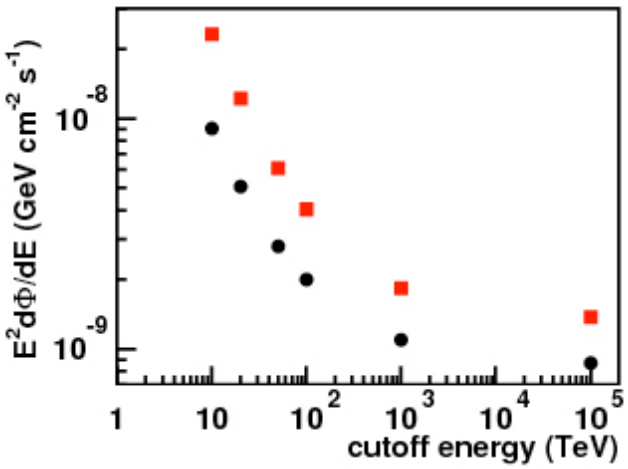

Figure 6-13: Evolution of the one year flux sensitivity (black dots) and discovery flux (5σ, 50% probability; red squares) for point sources at a declination of -60° as a function of the assumed cut-off of the energy spectrum.

The expected neutrino fluxes and the corresponding KM3NeT event rates from various Galactic high-energy gamma ray sources, observed by the HESS telescope, have previously been calculated assuming that the gamma emission is of purely hadronic origin, i.e. from π^0 decays [77]. This study has now been updated, using the most recent gamma flux measurements and the effective areas reported in this document. The results are presented in Table 6.1. Significant uncertainties arise from the fact that the gamma ray measurements do not precisely constrain the cut-off energy of the spectra, which are of central importance for the expected neutrino event numbers. For several sources, however, a significant detection after several years of observation time appears to be possible. This is confirmed by a dedicated study for RX J1713.7-3946 in which the source was simulated as an extended shell-type SNR. The study used a full Monte Carlo and analysis chain to determine the significance of the signal in the KM3NeT detector as a function of observation time (Figure 6-14).

Source Name	Source radius (°)	Visibility	Number of events for $E_\nu > 5$ TeV	
			Signal ν	Atm ν
RX J1713.7−3946	0.7	0.74	4 – 11	6.4
RX J0852.0−4622	1.0	0.84	2 – 6	17
Vela X	0.4	0.81	4 – 15	3.5
Crab Nebula	< 0.1	0.39	1 – 3	0.8

Table 6.1: Numbers of expected events in five years of observation time for a selection of possible Galactic sources of neutrinos. The numbers of signal events and of background events from atmospheric neutrinos inside the optimised cone cut is given. The source extension and the fraction of time the source is visible are also indicated.

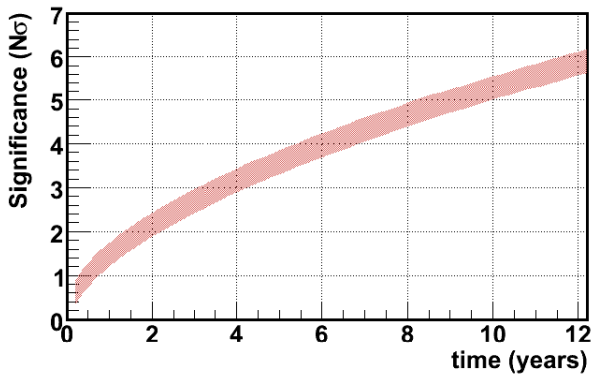

Figure 6 -14: Significance for discovery of supernova remnant RXJ1713 as a function of years of running time.

6.3.3 Transient Sources

For transient sources, it is possible to reduce the background dramatically by selecting a time window around the neutrino emission period. Different analysis techniques will be applied to objects like GRBs, AGN flares and microquasars, where information on the emission time is obtained from the observation of electromagnetic radiation, and to sources which have no emissions recorded by other instruments. To illustrate the performance of the KM3NeT detector, studies of GRBs and core-collapse supernovae are presented in the following. The two strategies used by ANTARES for the search of neutrinos coming from transient sources can also be applied for KM3NeT [78]. The first method is based on a search in conjunction with an accurate timing and positional information provided by external observations: the *Triggered Search*. For GRBs, the triggers are generated by a set of satellites sending signals to the Gamma Ray Burst Coordinates Network (GCN), which distributes the data of the GRBs detected by spacecraft. At the present time, GRB alerts are primarily provided by the Swift and FERMI satellites. For the future decade, several GRB missions have been proposed. One of the most advanced, with launch scheduled in 2012, is the

Space–based multi–band astronomical Variable Object Monitor (SVOM). The second search strategy exploits the very large field of view of a neutrino telescope and is based on multiplets of neutrino events coming from the same direction within a short time window: the *Rolling Search*. Gamma-ray bursts are the most energetic events in the Universe. Discovered in the late 1960s, their cosmological origin was unambiguously demonstrated only in 1997 when the first observation of a GRB afterglow provided a distance measurement. From the radiation flux on Earth, the typical gamma energy emitted by a GRB in a couple of minutes is estimated to be 10^{51}–10^{52} erg, depending on the collimation of the radiation flux. Observations suggest that the long-duration (>2 s) bursts originate probably from the collapse of a massive stellar progenitor into a black hole, whereas short-duration (<2 s) bursts progenitors, both lead to the formation of stellar black holes and collimated jet outflows. In the current canonical picture, the so-called *Fireball* model [79], "shells" of matter (plasma) are emitted from the vicinity of the new-born black hole into the interstellar medium with relativistic bulk Lorentz factors (typically >100). If shells with different velocities are emitted, a faster shell can reach a slower one and produce a shock which generates particle acceleration.
Using the Fireball model and measured gamma-ray spectra, it is possible to make predictions for the corresponding neutrino spectrum [80]. Figure 6-15 shows the neutrino energy spectrum calculated for a set of sample GRBs (see also [81]) detected by Swift and FERMI. Table 6.2 gives neutrino signals for the two most powerful bursts of Figure 6-15 plus the sum of 100 bursts according to a reference spectrum of Waxman and Bahcall [72]. It is clear that KM3NeT would be able to make a very significant discovery if these rates are correct. However, it has to be kept in mind that these predictions must be taken as order-of-magnitude estimates.
An example of the rolling strategy is the search for neutrino bursts from core-collapse supernovae. It has been suggested [83,48], that in some of these explosions the jet does not escape from the stellar environment and the gamma ray emission is "choked", so that the event cannot be observed by GRB satellites and only the neutrino emission is bright ("failed GRB").
In such models mildly relativistic jets ploughing through a star would be efficient in producing high energy neutrinos. The predicted neutrino spectrum follows a broken power law and for a supernova at a distance of 10 Mpc, about 60 events are

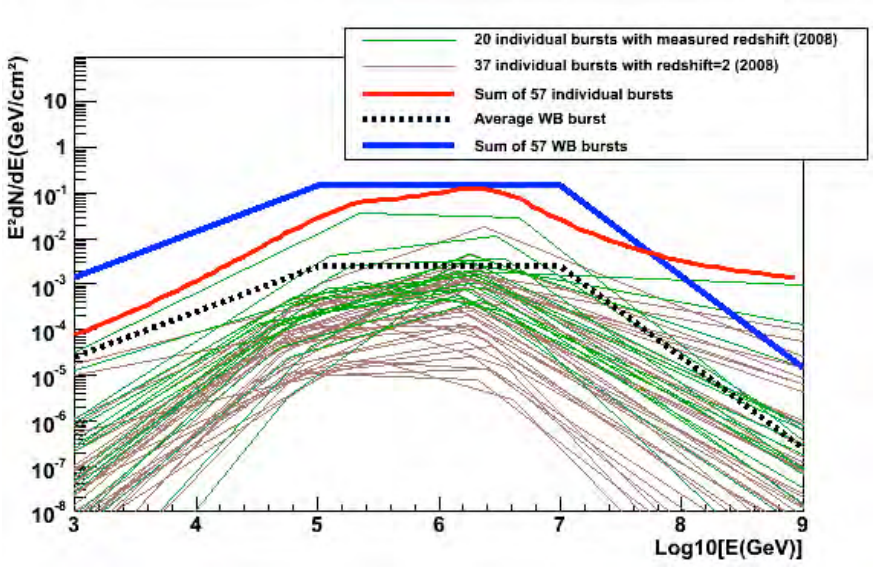

Figure 6-15: Neutrino spectra predicted for 57 GRBs detected in 2008 which could produce up-going events in the KM3NeT detector. The green lines indicate the expected neutrino fluxes for 20 GRBs with measured redshift, the brown lines the fluxes for 37 further GRBs without measured redshift, for which z=2 was assumed. The neutrino flux from an average GRB in the Waxmann Bahcall model [82] is indicated by the dashed black line. The sum of the individual GRB fluxes (green and brown lines) is shown as the red line, the sum of 57 average Waxman-Bahcall GRBs as the blue line.

neutrinos from the same celestial direction within a short time window. Within a distance of 10 Mpc, the rate of core-collapse supernovae is more than 1 yr^{-1} giving a high probability for the observation of such an event in the lifetime of the experiment. The basic idea of the rolling search method is that the detection of a small number of neutrinos in temporal and directional coincidence is statistically significant. For example, with KM3NeT, the probability of a random coincidence of three atmospheric neutrinos within a time window of Δ t=100 s and a solid angle of $\Delta\ \Omega = (2°)^2$ is $4x10^{-3}$/year. The method makes no assumption on the nature of the source and can be applied for any transient source of neutrinos.

At X-ray and lower gamma-ray energies, the sky is observed at any given time by modern space-based astronomical observatories like Swift and FERMI. Ground-based high-energy gamma-ray detectors like H.E.S.S. or MAGIC currently cover only a small fraction of the sky at any given moment. Multiwavelength astronomical observations can be used to associate neutrino point source detections with transient astronomical sources like AGN flares or jet-production events, thus significantly enhancing the discovery potential. Furthermore, it is possible to organise a follow-up programwith a small network of automated 0.3 - 1m telescopes, as originally proposed in [84]. Such optical telescopes already exist and many more are planned. For example, the TAROT network used by the ANTARES collaboration [85] and the ROTSE III network used by the IceCube collaboration[86], consist of several robotic telescopes, each with a 1.9° × 1.9° field of view.

GRB	Signal	Background
GRB080319B RX	2.6	5×10^{-4}
GRB080916C	2.7	5×10^{-4}
100 typical GRB	12	6×10^{-2}

Table 6.2: Number of expected signal and background events from the two most energetic GRBs detected by SWIFT (GRB080319B) and FERMI (GRB080916C) during 2008. Also shown is the sum of the signal expectations for 100 bursts (which roughly corresponds to the GRB detection rate per year with future satellite systems) according to the reference spectrum of Waxman and Bahcall [82].

6.3.4 Diffuse Fluxes

Beyond point-like sources, the following diffuse fluxes of neutrinos are expected:

- diffuse neutrino flux from unresolved extragalactic sources;
- cosmogenic neutrino flux produced during the propagation of ultra-high energy protons through the CMB radiation;
- a diffuse neutrino flux from the Galaxy.

Without the possibility of using a tight angular cut for reducing the background of atmospheric neutrinos, diffuse neutrino flux searches have to rely on a cut on the reconstructed energy. Such a cut is effective in separating cosmic neutrinos (with a spectrum expected to be roughly proportional to E^{-2}) from atmospheric neutrinos (spectrum proportional to about $E^{-3.7}$). In the case of a Galactic diffuse flux, directional information can be used for selecting events close to the Galactic Plane.

The energy reconstruction of neutrinos is based on the photon-counting capabilities of the detector. The energy loss of the final-state muon from charged current muon-neutrino events is, for muon energies above about 1 TeV, proportional to the muon energy. The number of detected photons is, in turn, proportional to the muon energy loss in the instrumented volume of detector. The neutrino energy is finally estimated from the muon energy, taking into account the kinematics of neutrino-nucleon interactions. For the present sensitivity studies, a simple energy estimator was used, based on hit counting for the reconstructed muon track. The neutrino energy resolution expected in KM3NeT for muon neutrino events is about $\Delta\log(E_\nu) = 0.5$.

A further difference between the atmospheric and cosmic neutrino fluxes which can be exploited in the analysis is the different composition in neutrino flavours. At high energies, the atmospheric neutrino flux mainly consists of ν_μ, while cosmic

flavours are distinct; for example, ν_e and most of ν_τ reactions induce shower-type events, the charged-current channel of muon neutrino interactions yields a muon-type event. For ultra-high neutrino energies, as expected e.g. for the cosmogenic neutrino flux, the Earth is opaque to neutrinos. In this case, neutrinos coming from the upper hemisphere have to be identified and separated from the atmospheric muon background. For such studies, shower events are important since they profit from a strongly reduced background induced by atmospheric muons. The sensitivity to diffuse neutrino fluxes presented here is based only on the ν_μ mode; a reconstruction of shower events is under study [87].

Diffuse Flux from Unresolved Extragalactic Sources

The cosmic rays above the "knee" of the spectrum at about 10^{15}eV are believed to have an extragalactic origin and are thought to originate from sources such as AGNs and GRBs. The neutrinos from a multitude of such objects are expected to form an isotropic, diffuse flux. Assuming that the proton energies in such cosmic ray sources is completely transferred to pions, which then produce neutrinos through their decays, one can derive an upper limit for the resulting extragalactic diffuse neutrino flux [88]. This is known as a "Waxman-Bahcall limit" and, for an E^{-2} spectrum, is equal to $E^{-2}\,dN/dE$ = 5 x 10^{-8} GeV cm^{-2} s^{-1} sr^{-1}.

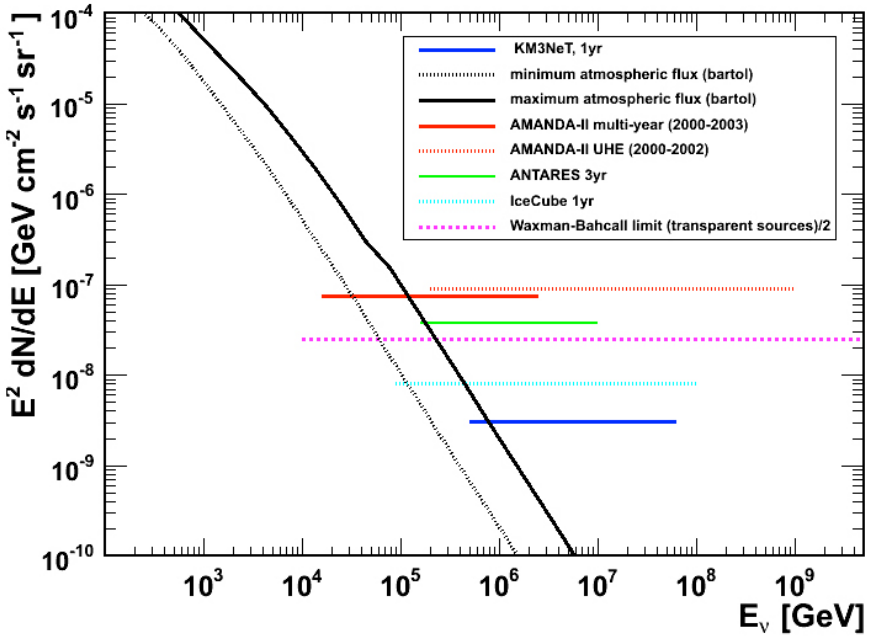

Figure 6-16: Diffuse flux sensitivity of the KM3NeT neutrino telescope for one year of observation time, together with Waxman-Bahcall limit [88] and sensitivity limits from AMANDA [89,90], ANTARES [91 and IceCube [92]: recent preliminary results from the 40 line IceCube detector show that these predicted limits have already been reached. For the experimental sensitivities, the horizontal extent of the limit lines indicates the energy range for which the study was performed.

The sensitivity to diffuse fluxes was optimised with the MRF method leading to an effective energy cut $E_\nu > 10^{5.6}$ GeV.
A neutrino flux with a spectrum proportional to E^{-2} was assumed. The minimal flux limit obtained is 3x10^{-9} GeV cm^{-2} s^{-1}sr^{-1} and is shown in Figure 6-16 together with results obtained for other neutrino telescopes.

Cosmogenic Neutrino Flux

A diffuse "cosmogenic" neutrino flux is generated during the propagation of cosmic rays through the cosmic microwave background radiation (CMB). Above about $10^{19.6}$ eV the cosmic ray protons produce pions through photo-production of Δ resonances: $p\gamma_{CMB} \rightarrow \Delta^{+} \rightarrow n\pi^{+}/p\pi^{0}$. The subsequent decay of the charged pions and neutrons results in a diffuse neutrino flux. For different cosmic ray compositions, the event rates per km^3 of water volume and per year are given in [93]. An estimate of the cosmogenic neutrino events rates in KM3NeT gives 2-3 events/year, assuming that all ultra-high energy cosmic rays are protons.

Galactic Neutrino Flux

The bulk of cosmic rays observed on Earth are produced in the Galaxy. The diffuse gamma and neutrino fluxes, which are produced in the interaction of cosmic ray protons and nuclei with the interstellar gas in the Galaxy, are expected to be roughly equal. The assumption that observed Galactic gamma emission comes from hadronic processes thus yields an estimate of the diffuse Galactic neutrino flux.

The Galactic plane occupies a relatively small area of sky, the inner part of which is visible from the Mediterranean Sea. This region has an extension of 0.097 steradians ($-40° < l < 40°$ and $-2° < b < 2°$, where l and b are Galactic longitude and latitude) and occupies less than 1% of the neutrino sky visible by KM3NeT.

The prediction used here for the neutrino flux was calculated from the multi-TeV gamma emission observed by MILAGRO [94]. The calculation assumes that the flux measured in the region $30°<l<65°$ is representative for the whole Galaxy (the inner part of the Galaxy was not visible to MILAGRO) and that the origin of this emission is entirely hadronic. The predicted event rates from the resulting Galactic diffuse neutrino flux in KM3NeT are given in Figure 6-17 for the three different cosmic ray spectra defined in reference [95]. Between 14 and 39 neutrino events are expected above 10 TeV in one year, depending on the cosmic ray spectra. The rate of atmospheric neutrinos under similar conditions corresponds to 80 events per year.

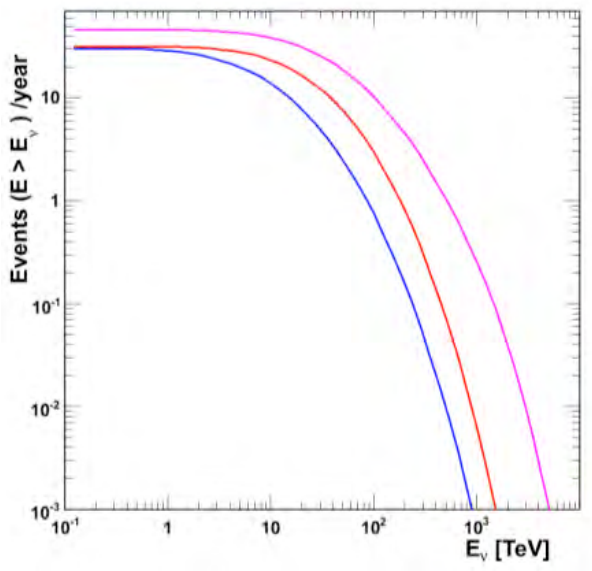

Figure 6-17: Integral neutrino event rates above a given energy in the KM3NeT neutrino telescope from the diffuse flux from the inner Galaxy; the three lines are the predictions for the different flux assumptions given [95]. About 80 atmospheric neutrino events are expected above 10 TeV.

6.3.5 Dark Matter

A deep-sea neutrino telescope allows for performing indirect search for Dark Matter, the existence of which is strongly indicated by astronomical observations and essential for the standard model of cosmology. Except in more exotic scenarios, Dark Matter is assumed to consist of neutral, weakly interacting massive particles (WIMPs) with masses of at least several GeV/c^2. Many theories, most notably Supersymmetry and Extra-Dimensions, feature a suitable candidate particle, which is stable due to conservation of a multiplicative quantum number that is different for Dark Matter and Standard Model particles. However, the annihilation of two Dark Matter particles into Standard Model particles is allowed. The Dark Matter is assumed to have frozen out of equilibrium with the lighter standard matter when the Universe cooled down. From measurements of the fluctuations of the Cosmic Microwave Background by the WMAP experiment, the current relic density of Dark Matter is derived, which poses strong constraints on the combination of mass and production/annihilation cross-section of the Dark Matter particles, independent of the specific theory [96].

Among the supersymmetric theories the minimal Supergravity model (mSugra) is especially well studied. In mSugra, the supersymmetry breaking occurs in the hidden sector and is communicated to the physical sector by gravity. Using the renormalisation group equation, the masses and couplings at the electroweak scale are calculated from four continuous parameters plus a sign defined at an energy scale of 10^{16} GeV. A valid candidate for Dark Matter could be the lightest of four neutralinos, which are the mass eigenstates of the four neutral higgsinos and gauginos.

The detection rate in KM3NeT of neutrinos originating from the annihilation of neutralinos captured in the Sun has been calculated for about four million distinct parameter combinations in the mSugra parameter space using DarkSUSY [97]. The scan was guided by comparison of the resulting relic density to the result from WMAP [96]. The ISASUGRA renormalisation group equation code [98] was used. For the Galactic halo profile, the Navarro-Frenk-White [99] parameterisation was chosen, and the mass of the top quark was set to 172.5 GeV/c^2.

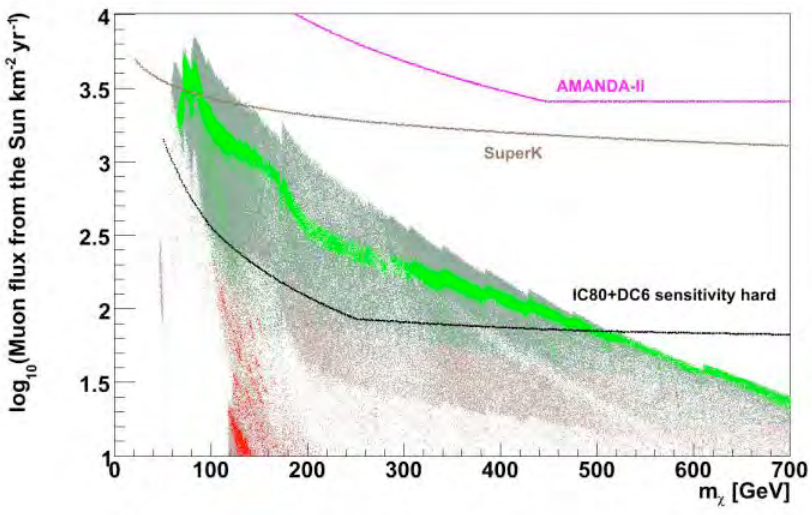

Figure 6-18: The muon flux above a threshold energy of one GeV induced in a neutrino telescope by neutrinos from annihilation of mSugra Dark Matter in the Sun, as a function of the neutralino mass The coloured points correspond to mSugra parameters consistent with the WMAP observations (see text). The models within (outside) the detection reach of KM3NeT are coloured green (red). The KM3NeT and IceCube sensitivities correspond to observation times of 10 years. Limits from selected experiments [100,103,102] are also indicated.

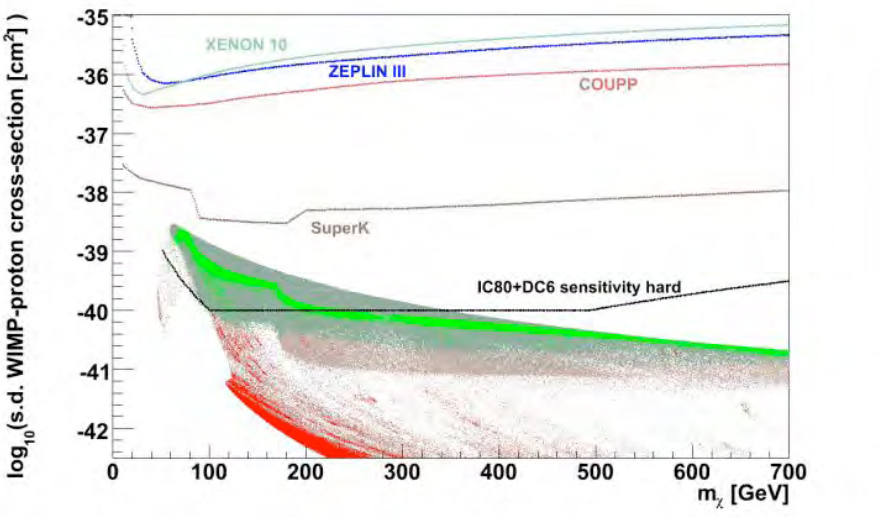

Figure 6-19: The spin-dependent WIMP-proton cross section plotted against the neutralino mass. The coloured points correspond to mSugra parameters consistent with the WMAP observations (see text). The models within (beyond) the discovery reach of KM3NeT are coloured green (red). Limits of selected experiments are also indicated.

From the detection rate for neutrinos originating from neutralino annihilation in the Sun, a 90% CL exclusion sensitivity for 10 years of data taking data was calculated. The analysis assumed a search cone of 3° radius around the Sun and the neutrino energy was restricted to be between 50 GeV and the mass of the neutralino. Detectable models are coloured green in Figure 6-18 and Figure 6-19, the others red. Bright colours indicate a relic density within the 2-sigma band of WMAP. The topmost branch of mSugra models corresponds to the Focus Point Region [104] of the parameter space. This region can be nearly completely assessed by KM3NeT. As seen from Figure 6-19, the sensitivity of KM3NeT on the spin-dependent WIMP-proton cross section is significantly higher than for current direct detection experiments [105,106,107], when measuring exclusively this quantity.

Comparing the IceCube experiment sensitivity [103], calculated under conservative assumptions, to the model-specific sensitivity of KM3NeT (Figure 6-18 and Figure 6-19), it can be concluded that IceCube's capabilities concerning Dark Matter detection will exceed those of KM3NeT. This is mostly due to the extra sensitivity added to IceCube by the "Deep Core" installation. Note that a similar set-up is also possible for KM3NeT and might be quickly installed in case findings from other experiments (IceCube, direct WIMP searches, LHC) suggest that this was appropriate.

7. Ecological Impact and Decommissioning

The environmental impact of the telescope infrastructure can be considered in the 4 time phases:
Phase 1: Construction and commissioning.
Phase 2: Operations and maintenance.
Phase 3: Decommissioning.
Phase 4: Legacy post-decommissioning.
Within each of these phases (to varying degrees) there are considerations regarding:
1. Shore-based infrastructure directly connected to the telescope.
2. Sub-sea infrastructure
3. The cable route.
4. Infrastructure and operations at the partner institutions.
5. Operations during manufacture at partner institutions and suppliers.

7.1 Construction and Commissioning

In general it is during this phase that the greatest environmental disturbance will occur associated with manufacture of the telescope components, their transport to the ultimate location and deployment in the sea. Once commissioned, the shore-based infrastructure connected to the telescope is modest in size comprising power supply systems and computers, which at the three main candidate sites can be accommodated in existing buildings. Therefore no major new construction works are anticipated on shore. The sea floor infrastructure implies assembly of a large weight and volume of material. For transportation it is expected that material will be containerised and total quantity will be of the order of 1000 Twenty-foot Equivalent Units (1000 TEU). This represents a small fraction of the annual traffic at regional ports Marseilles 0.8mTEU, Gioa-Tauro 3m TEU and Piraeus 1.6m TEU[108] and will be spread over several years of construction. Locations will be sought for final assembly and testing before loading onto the deployment vessels. Since distances in the Mediterranean Sea are short, such integration can be done at any convenient port location. Localised impact at the telescope site will be minimal.
During construction deployment vessels will occupy the water over the telescope site. Navigation by other shipping will be controlled by issuance of Notices to Mariners and display of appropriate shapes and lights under the IMO (International Maritime Organisation), Convention on the International Regulations for Preventing Collisions at Sea, 1972 (COLREGs). This will be carried out in consultation with local fishing and shipping interests and the guidance of relevant national coastguards. Deployment of the sub sea infrastructure itself is expected to have negligible impact.
Laying of the cable from the shore to the deep sea infrastructure raises issues of way- leaves for the cable through the littoral zone and possible need for trenching or cover to protect from anchoring and fishing until an appropriate depth is reached. Well-established best practice for cable and pipeline laying in the Mediterranean area will be followed

7.2 Operations and Maintenance

During normal operations of the telescope there will be no evidence of presence of the system on the surface. The top of the optical strings or towers will be more than 1500 m below the sea surface beyond the depths of concern for navigation by surface vessels, normal fishing gears or military submarines (maximum depths are classified but are specified as no more than 250 m). However fishing vessels in the Mediterranean Sea do deploy baited long lines or gill nets which may be more than 1500 m long and although intended to be deployed near the surface may sink deeper during shooting or recovery. Limitations on fishing activity over the array may be a prudent measure.
The system will occupy a volume of sea water of several cubic km and may form an obstruction to movements of large animals. There is life at all depths in the Mediterranean Sea but particularly the Eastern basin is considered oligotrophic (low productivity) and abundance of animal life is much lower than in e.g. the North Atlantic Ocean.

The maximum depth at which large sharks have been observed in the Eastern Mediterranean Sea is 2500 m[109] with only relatively smaller fishes and shrimps occurring at greater depths. The world record for the dive depth of whale was recorded in the Mediterranean Sea as 1900 m[110]. Depending on depth of location of the telescope infrastructure it is therefore possible that interactions may occur at the top of array with large animals such as whales and sharks. The array will emit sound and light from its test beacons which will be detectable by marine fauna. The acoustic frequencies used >10kHz are inaudible to fishes but will be detectable by marine mammals at close range. Most deep-sea animals can detect light in the blue part of the spectrum around 480 nm. There is the theoretical possibility that these animals may detect and reply to beacon signals. Sharks have electromagnetic sensors and may be able to detect switching of currents in the power supplies. The main biological effect of the array is that it will provide areas of hard substrate in an otherwise fluid environment upon which some species of organisms can settle and grow[111]. Whilst this provides opportunities for such organisms, this is considered to be undesirable fouling growth for operation of any underwater equipment. Fouling begins with a film of bacteria coating the equipment followed by colonisation by various sessile animals species such as sponges, corals and barnacles depending on the availability of source larvae. Trials so far indicate rates of fouling at the great depths proposed will be low but limited use of approved antifouling materials may be necessary on key components. From time to time the sub sea infrastructure may require maintenance interventions. Ships with remotely operated vehicles will then need to occupy the site.

7.3 Decommissioning

The intention is that buildings on shore will be reallocated for other uses. For the subsea components, KM3NeT will comply with UNCLOS1 – 1982 United Nations Convention on the Law of the Sea Article 60(3) which includes the following text *"Any installations or structures which are abandoned or disused shall be removed to ensure safety of navigation, taking into account any generally accepted international standards established in this regard by the competent international organisation. Such removal shall also have due regard to fishing, the protection of the marine environment and the rights and duties of other States. Appropriate publicity shall be given to the depth, position and dimensions of any installations or structures not entirely removed"*

Generally the KM3NeT infrastructure is too deep to be of concern for navigation or fishing. Decommission of offshore structures is generally governed by the United Nations Environment Programme (UNEP) and in the Mediterranean Sea KM3NeT should comply with the relevant UNEP regional seas agreement which is the Barcelona Convention, Convention for the Protection of the Marine Environment and the Coastal Region of the Mediterranean (Revised 1995)
All the sub-sea components above the sea floor will be cut off and removed to shore for disposal in accordance with the Barcelona Convention. In view of the great depth, inert ballast blocks and cables will be left in place; it is considered that the disturbance created by attempting to remove material which by this time will be encrusted with growth, covered in sediment and settled into the sea floor would be detrimental to the environment. Any cable exposed at less than 1500m depth will be cut off and removed to restore the sea floor to original condition for access by fishermen.
Cost of decommissioning will be included in the business plan for the infrastructure.

7.4 Legacy Post-Decommissioning

Following decommissioning there will be very little evidence of that the infrastructure was ever there. The precise locations of material, on the sea floor (bases of strings) will be lodged with international marine data centres and may form the basis for future investigations of marine processes on materials deployed at a known time in the past for comparison with the emerging field of deep sea archaeology in the Mediterranean Sea.

8. Quality Assurance and Reliability

The KM3NeT infrastructure must operate for at least 10 years, without significant degradation, at a depth of up to 5000 metres (50 MPa pressure) in the chemically-aggressive deep-sea environment. This imposes strict quality standards on each subsystem within the detector. To meet these standards a quality assurance system will be implemented covering each step of the detector production, transportation, deployment and operations.

During construction and operation, there is a need for:

1. Well defined actions for coordination, planning and control.

2. Identification of weak points in the design and operation of the detector and the subsequent corrective and mitigating actions through design improvements and operational procedures.

The quality assurance system requires the implementation of a management structure, the identification of responsibilities and resources, and the definition of procedures and activities.

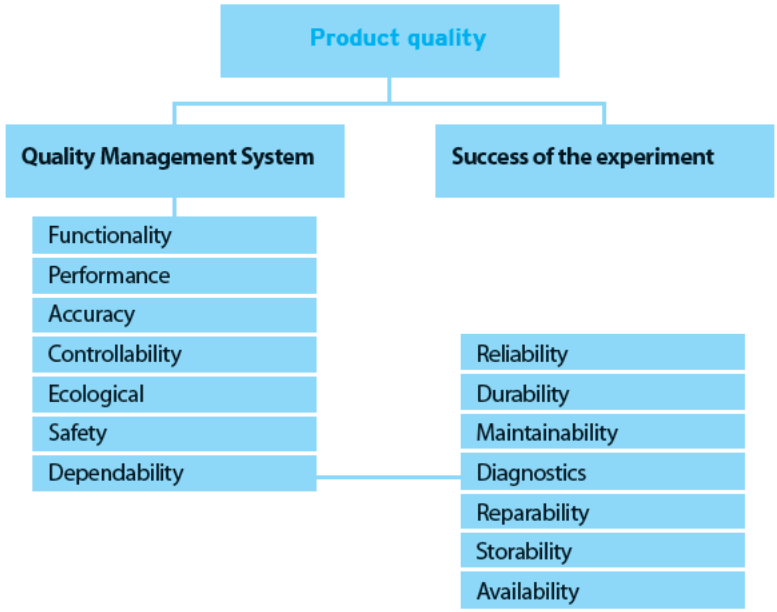

Figure 8-1: Schematic structure of product quality. [112]

A schematic structure of a generic product quality system is shown in Figure 8-1. It shows the link between quality and reliability of a product.

In the following the quality management system will be described based on an adopted methodology and risk and dependability analyses.

8.1 Methodology

Several different quality standards have been analysed. The choice has fallen on the ISO 9000 family of standards. It is widely adopted in industry and allows the freedom to customize the standard to the specific KM3NeT requirements.

The Quality Management System (QMS) must address the requirements of quality assurance (QA) and risk assessment (RA). It includes the quality control process through the Deming cycle, a design optimisation process, and allows for the risk analysis to proceed in parallel and interact with the design.

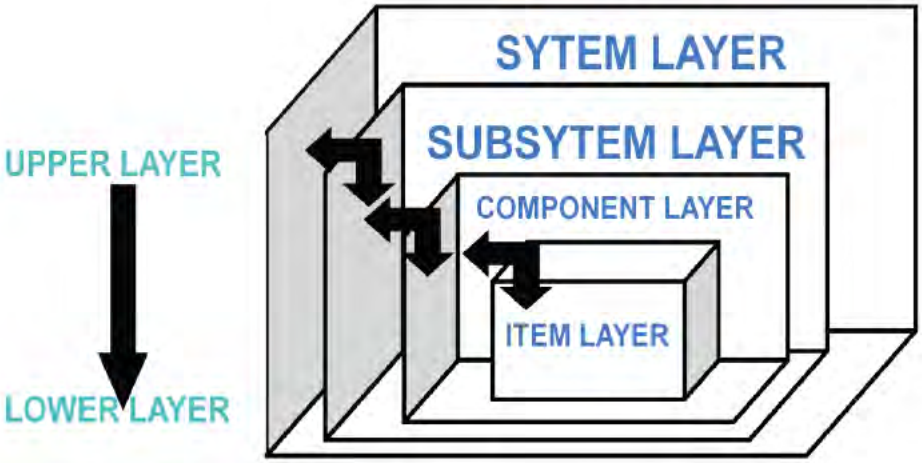

Figure 8-2: KM3NeT schematic logic scheme.

Following the ISO 9001 standard KM3NeT is described in terms of processes. The detector is represented by a logic scheme presented in Figure 8-2. Such a scheme enables the unique identification and traceability of components and describes their dependability. Within the framework of KM3NeT, the quality assurance and risk analysis are coupled to form an integrated system as shown in Figure 8-3.

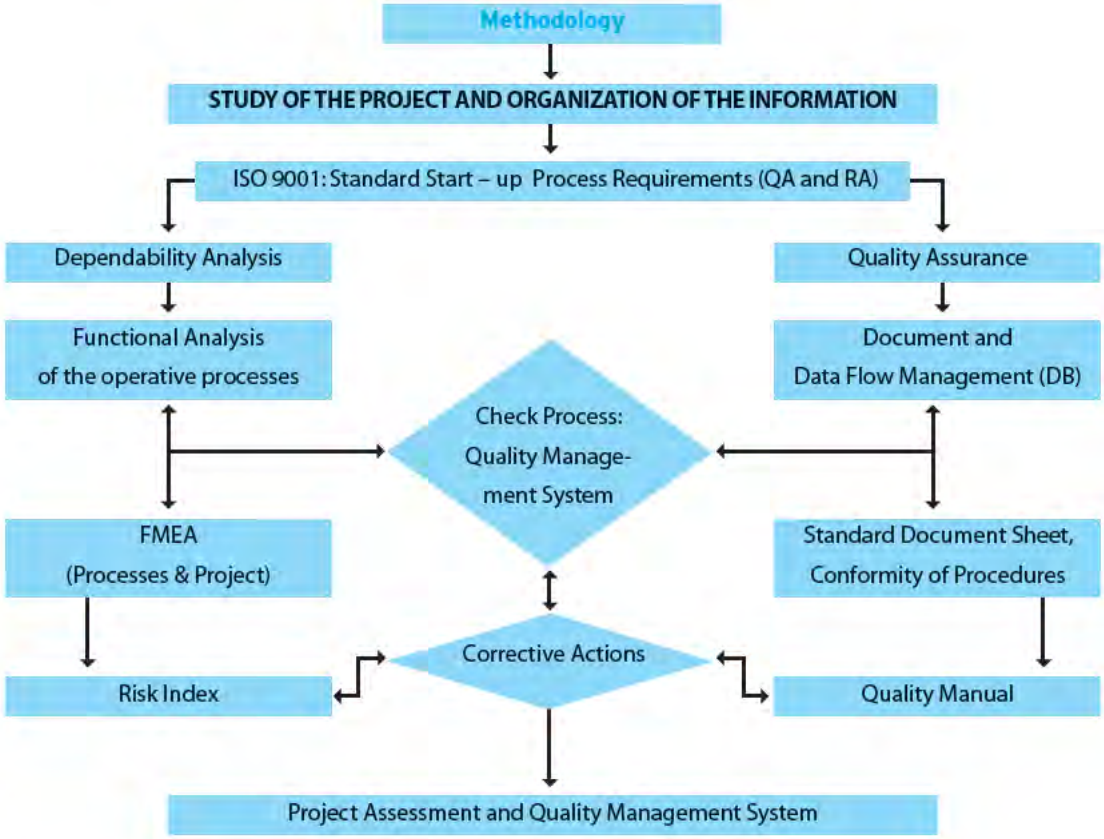

Figure 8-3: Schematic structure of the Deming cycle methodology Plan, Do, Check, Act.

In particular it has been translated into:

- An in depth study of the project, based on information from the pilot projects and the general requirements formulated in the KM3NeT design study.
- An organization of the collected information
- The analysis of QA and RA standards;
- The development of the QA and RA systems in parallel
- The monitoring of design activities;
- Identification of weak points and subsequent corrective actions.

The implementation has used questionnaires and audits for information gathering. The system functionality has been described in flow and block diagrams and a product breakdown structure has been defined.

8.2 Quality Management System

The QMS must take into account the complexity of KM3NeT not only in terms of number of components and systems but also in terms of the international nature of the consortium.

The QMS is modular and hierarchical as indicated in Figure 8-4. The quality assurance rules are passed down the structure and at each stage further restrictions and rules can easily be added. As far as possible the general structure of QMS should be respected.

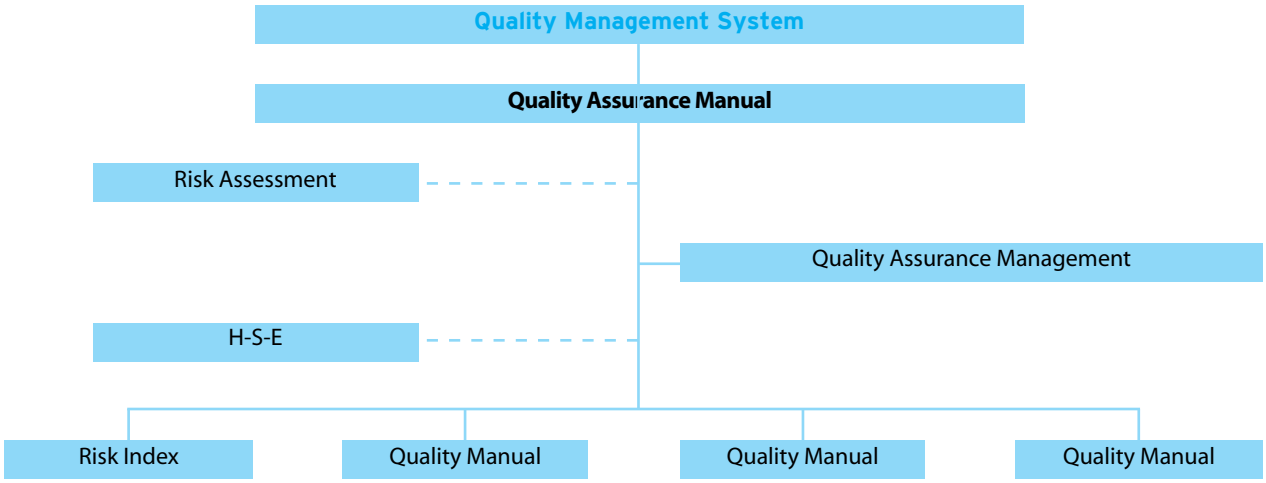

Figure 8-4: KM3NeT quality management system.

8.2.1 Quality Assurance Manual

The quality assurance manual describes the general structure of the QMS. It details the objectives of the project and the structure of the project management. It defines the quality policy and the quality documentation including reference documents, quality management documentation (QMD), procedures, quality plans and the quality management database.

The quality assurance is closely interwoven with risk assessment, both in terms of risk management and dependability analysis, and health, safety and environmental issues.

The risk assessment provides input to the design review process and the quality control actions to be taken to avoid and mitigate weak points. The analysis of health, safety and environmental issues provides input into the QMS procedures ensuring they comply with European and national laws. In each phase of the project, the quality assurance manual needs to be reviewed and updated where necessary.

Quality Assurance Management

The structure of the management is given in Figure 8-5. The overall management of the quality assurance is contained in the quality executive. It comprises a number of managers that are responsible for different aspects of quality control. The executive is in charge of:

- The management of the QMS;
- The definition of procedures and quality control actions in close cooperation with the experiment executive and technical experts;
- The internal and external quality auditing;
- The organisation of periodic quality assurance training courses.

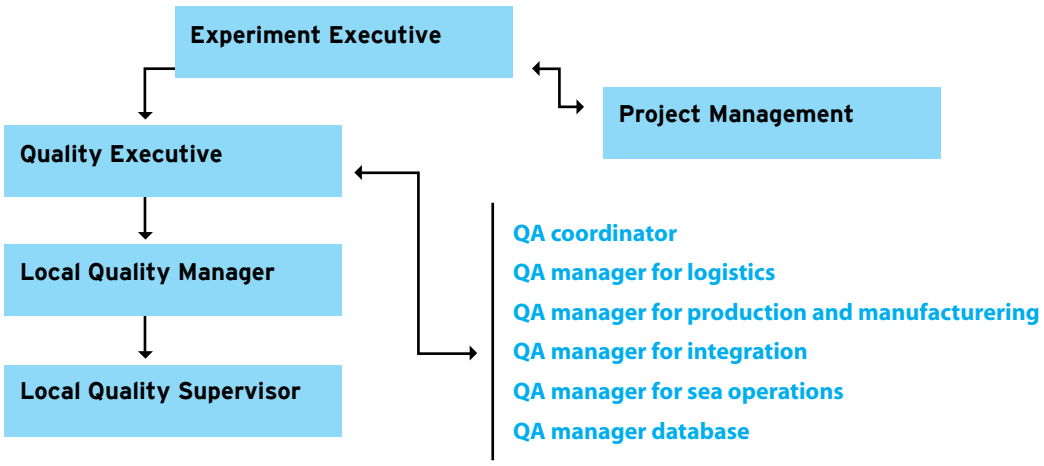

Figure 8-5: KM3NeT quality management.

The managers that comprise the executive are the following:

- The coordinator: the representative of the quality office in the steering committee;
- The logistics manager: oversees the packaging, storage and transportations;
- The production manager: oversees the communication of quality requirement to suppliers and defines and monitors acceptance tests;
- The integration manager: oversees the quality aspects of design integration and operation;
- The sea operations manager: oversees quality and health and safety during all sea operation activities;
- The quality assurance database manager: manages the QMS database.

The managers of the executive will define the quality assurance procedures in their individual areas of responsibility. Figure 8-6 shows some of these areas that will require procedure definition. This process is dynamic and the procedures will require continuous review and update.

Specific items such as optical modules, storeys, detection units and deployment operations will require customized quality plans. These are similar to those developed for and applied in the ANTARES and NEMO pilot projects. These will require the coordination of several quality managers.
At the local level the executive is represented by a local quality manager, responsible for all aspects of the QMS within his institute on a day to day basis, and a local quality supervisor, responsible for the quality control and application of the QMS in a specific area.

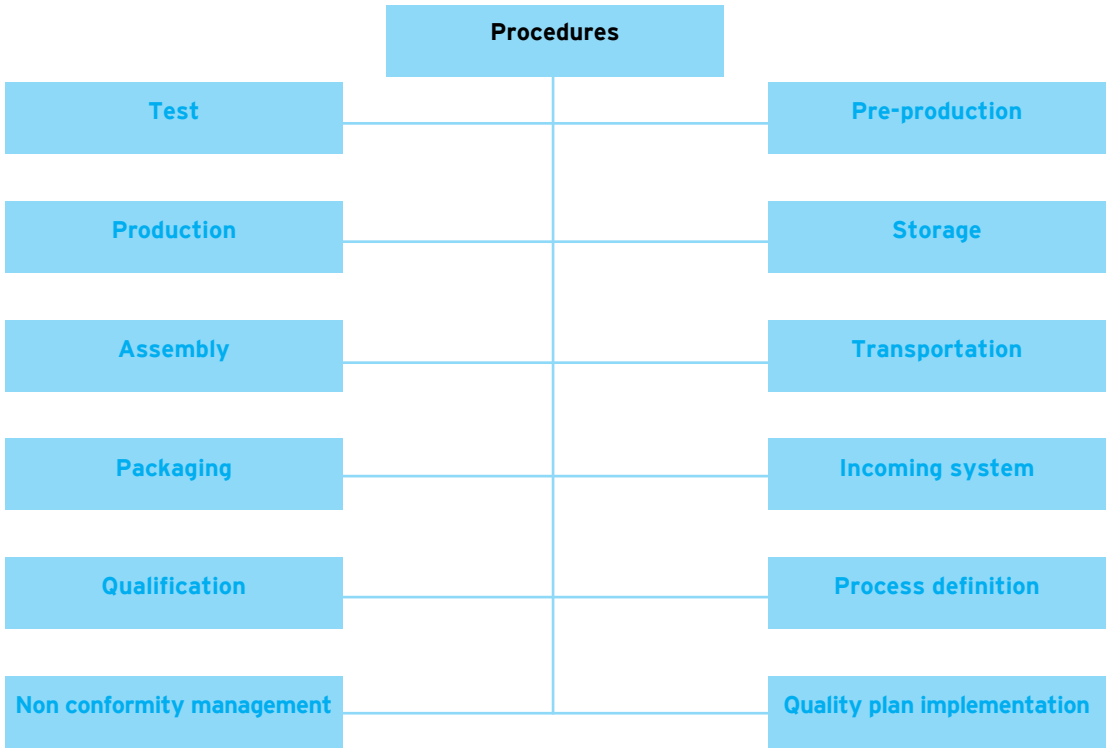

Figure 8-6: KM3NeT procedures.

Quality management documentation
Rules have been defined for the identification of documentation and components within the system.
For the documentation these include an identification number, categorization, validation by the appropriate quality assurance manager and an up to date history of the document.
For the components it comprises a product breakdown structure along the lines of the scheme presented in Figure 8-3.
Finally a naming convention has been developed.

Database
The documentation database design relies on the experience gained with such databases in the pilot projects. The requirements for the KM3NeT database have been defined and a prototype was developed. It includes on-line access to test records and the definition of the product breakdown structure.

It maintains document, component and system traceability during the qualification, construction and operation phases of KM3NeT.
It is modular and based on the product break down structure, as shown in Figure 8-7 and will contain the entire technical documentation.
The history and traceability of all the components and systems are contained in the storage module. Information on integration and deployment is stored in the respective modules and the current status of all deployed component is contained in the layout module. All modules are interlinked and are accessible through user interfaces.
The layout module is the interface in the control room. It provides all the technical information on the components deployed and running on the sea bed.

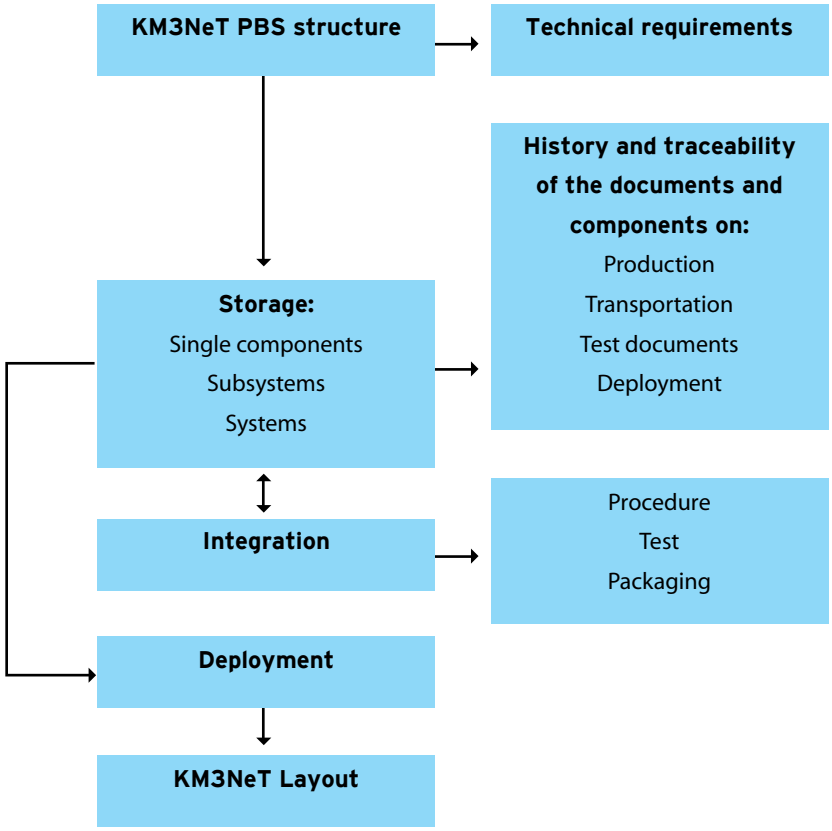

Figure 8-7: KM3NeT database structure.

8.3 Risk Assessment

In complex, expensive, unique or one-of-a-kind systems, like the neutrino telescope, assessment of the mechanisms of potential failures through analysis is a necessary ingredient of risk analysis because a statistical basis for the overall system performance is not available. Risk must therefore be synthesized from information about the performance of simpler subsystems or components of the system. This information comes either from past operational experience in other systems or through experimentation. The objectives of a risk analysis for KM3NeT are therefore

1. To define the mission of the neutrino telescope in quantifiable terms

2. Assess specific scenarios (sequences of events) that can lead to the inability of the system to perform its mission

3. Assess the probability of each and every scenario

In this sense a risk analysis results in a set of triplets $\{s_i,pi,ci\}$ providing specific scenarios (si) with their associated probability of occurrence (p_i) and consequence (c_i). Risk representation with the set of triplets provides more information and enables risk management decision making since it differentiates among different types of failures in terms of their severity and their relative probability. In reliability analyses it is customary to define only one type of consequence (e.g. mission failure) and then calculate only the probability of occurrence of the various paths that lead to it. This implies that all types of mission failure are equally important, which may not always be the case.

The risk analysis, described in the CDR [1], essentially entails the determination of the values for (s_i), (c_i) and (p_i). The first two can be obtained by a qualitative analysis of the full detector system, whereas the third is obtained from a quantitative analysis based on existing reliability figures obtained from pilot projects, results from accelerated testing of components or manufacturers data.

8.4 Dependability analysis

The dependability analysis is used in KM3NeT mainly as a "technological system". It assumes that the detector has been constructed and is operating. The analysis developed allows correlations between the reliability characteristics of the components and those of the total system to be made.

A first order approximation to the dependability analysis of the design of the neutrino telescope has been conducted. System availability criteria are generated from the existing functional and performance requirements, defined in the CDR. In terms of risk analysis a system, or component, is deemed available when it operates in excess of a predefined operational threshold.

For a complex system, availability of the system depends on the availability of the components. The first problem to be addressed in dependability analyses is the calculation of system availability as a function of component availabilities. The system performance can then be viewed from two different perspectives.

- Given the availabilities of all the components of the system, determine the availability of the system as a whole.
- Given a performance criterion or required function, expressed as a system availability level, determine the component availabilities that will satisfy this criterion.

Fundamental to the dependability analysis of any system, is the definition of its required function. The primary function of the neutrino telescope is to allow for the recording and analysis of tracks produced in the interaction of neutrino. The essential component in determining the telescope availability is the optical module. The optical module availability includes not only the optical module operability but also its ability to transport data back to shore. It is then reasonable to define the required function of the telescope to be a minimum number of available optical modules in the telescope. An additional requirement is that the telescope is available for a percentage of its useful life (10 years).

The large volume neutrino telescope consists of various components and subsystems that can be divided into three major subsystems:

- The detector network, from optical module to primary junction box;
- The deep-sea infrastructure, primary junction box to shore;
- The on-shore infrastructure.

All three subsystems must operate for the telescope to be available. Hence they are logically connected in series. The on-shore infrastructure subsystem was not included in this phase of the dependability analysis, since repairs of this system can be performed instantaneously.

The overall unavailability of the neutrino telescope is then a function of the unavailability of the detector network and the unavailability of the deep-sea infrastructure. The latter is easily evaluated as the combined unavailability of the primary junction box(es) and the main electro-optical cable(s) to shore.

The model developed for the calculation of the detector network unavailability was based on the method of successive decomposition. The detector network comprises the optical modules on the detection units, and the junction boxes for each detection unit, branch and sector. If a sector junction box or the associated cabling to the main junction box fails then all optical modules mounted in the detection units of the branches in this sector become unavailable. Similarly if the junction box of a branch or the cabling connecting it to the sector junction box fails then the optical modules of the detection units in this branch become unavailable. Finally if the junction box of a detection unit or the cabling connecting the detection unit to the branch junction box fails or the detection unit itself fails structurally then the optical modules of this detection unit become unavailable. Figure 8-8 gives the block diagrams at each decomposition level, illustrating the development of the unavailability model. It is a generic many level representation and allows for intermediate levels to be absent, if required by the design. On the basis of these observations and a detector function based on the minimum number of available optical modules, the detector network unavailability is calculated. Detailed information on the development of the unavailability model can be found in [113].

The developed unavailability model provides the combined unavailability of the detection network and the deep sea infrastructure based on component unavailability. As a first approximation the steady state dependability of the system was calculated. This means that the availability of each of its components is set equal to the mean availability over the life time of the system. The steady-state unavailability for all components was calculated. The assumptions made at this stage include:

a) parts of the detector are designed in such a way that they are retrievable, serviceable and replaceable;
b) failure of a component is immediately detectable;
c) repair starts immediately or only at predetermined intervals;

The different components were classified into two classes:

a) those that are retrievable and repairable
b) those that are not repairable

The risk analysis considered the two distinct approaches followed by the project. One being a design with extended storeys incorporating six optical modules with large PMTs (simulating the bar and triangle design) and the other being the string design with multi-PMT optical modules.

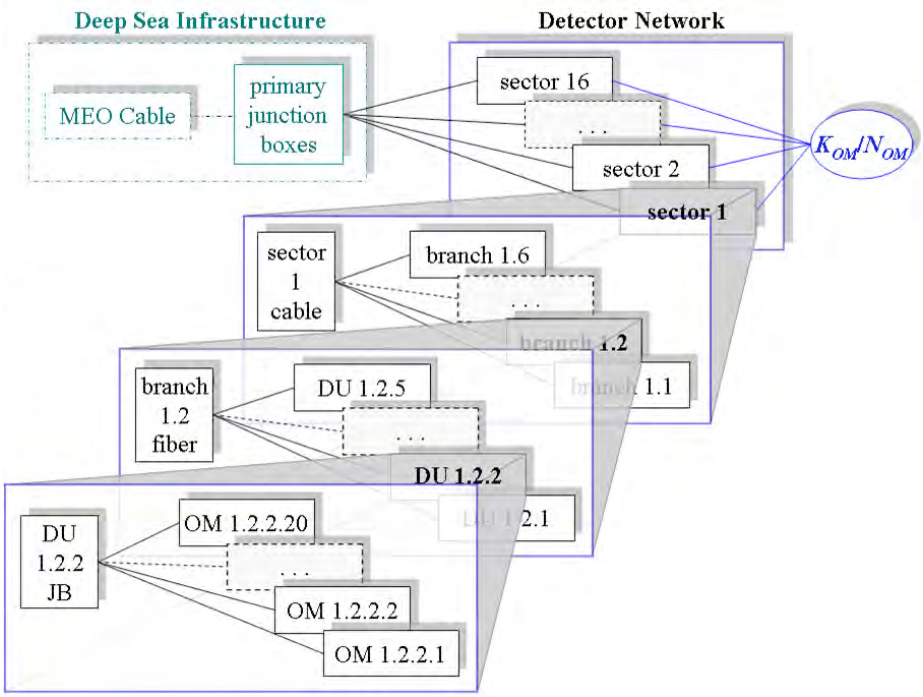

Figure 8-8: Generic detector network and deep sea infrastructure block diagrams.

For both case studies the cables connecting the detection units to the secondary junction boxes, those connecting secondary boxes to primary junction box and the cable running from primary junction box to shore are instantly repairable and the repair period is one month. The primary junction box is repairable. For the secondary junction boxes both instant reparability and non-reparability are investigated.

- For the extended storey design, the optical modules, the storeys and the detection units are either non-repairable or repairable with a repair period of one month and a maximum number of repairs per year of 12. The detector has a hexagonal layout and the design has 15240 optical modules and 2540 electronic modules.
- For the string design the optical modules and the detection units are non-repairable. The detector has a hexagonal layout and the design has 6200 optical modules.

A number of sensitivity analyses were performed on the two alternatives. A variety of detector network layouts were considered to investigate the tradeoffs in the total number of optical modules and their arrangement. The detailed results of the dependability analysis are reported elsewhere [113]. The results enable estimation of the trade-offs between the component mean time to failure (MTTF), the component reparability and the required availability over a 10 year period. The system availability criterion was set to 90% of optical modules available over a 10 year period. It should be noted that the actual effort of achieving a particular MTTF or performing the repair of a component within the same or different designs might vary significantly.

These practical issues are not addressed in the present work due to lack of data. Therefore the results can not be, as yet, used to compare the two alternative designs. This analysis, however, does allow for optimisation of the configuration of each of the two approaches considered..

8.4.1 Results of the dependability analysis

Since designs are under qualification and optimization process the results and the configurations of the case studies will be according modified. As present status the following reports the results related to the analysis applied to the extended storey design in the configuration as described in chapter 3. It provides the magnitude of the MTTF foreseen for the detector and its components.

Two different approaches to achieve the defined unavailability of the system are presented:

- The MTTF value can be reduced applying maintenance strategy,
- If this MTTF is not technically achievable or too expensive the required extra unavailability can be provided by extra redundancy in the number of detection units and hence the OMs.

Results of the dependability analysis: maintenance and reparability of components

The following describe the trade-offs between the various repair schemes, the unavailability targets and the component MTTF. For instance, consider that all the components of the Deep Sea Infrastructure (DSI) have a MTTF equal to 10 years and are immediately repairable with mean time to repair (MTTR) equal to one month. The MTTF, (assumed equal for all components) required to achieve a given system availability is calculated. Table 8-1 gives the results of the dependability analysis for the following cases, where c represents the system operability criterion and U_{max} the maximum telescope unavailability.

In the first case,the PJB-SJB cables, the SJBs, the detection units, the storeys and the optical modules are non-repairable:.

For c=10%, as the unavailability target increases from 5% to 20%, the required MTTFs for the non-repairable components decrease by 40%. For c=20% the observed decrease is at 35%. As c increases from 10% to 20%, the average reduction in MTTF

Case 1: C=10%, DSI: MTTF=10yrs, MTTR=1month

		SJB		DU		cable, STO, OM
U_{Max}	%	MTTF [yrs]	MTTF [yrs]	MDT [month]	MTTF [yrs]	MDT [month]
Case 1	5%	600	Non-rep	600	Non-rep	600
	10%	450	Non-rep	450	Non-rep	450
	20%	360	Non-rep	360	Non-rep	360
Case 2	5%	11	1,2	630	Non-rep	630
	10%	11	1,2	430	Non-rep	430
	20%	11	1,2	330	Non-rep	330
Case 3	5%	11	1,2	21	2,2	630
	10%	11	1,2	21	2,2	370
	20%	11	1,2	21	2,2	280

Case 2: C=20%, DSI: MTTF=10yrs, MTTR=1month

		SJB		DU		cable, STO, OM
U_{Max}	%	MTTF [yrs]	MDT [month]	MTTF [yrs]	MDT [month]	MTTF [yrs]
Case 1	5%	235	Non-rep	235	Non-rep	235
	10%	182	Non-rep	182	Non-rep	182
	20%	152	Non-rep	152	Non-rep	152
Case 2	5%	11	1,2	185	Non-rep	185
	10%	11	1,2	153	Non-rep	153
	20%	11	1,2	123	Non-rep	123
Case 3	5%	11	1,2	21	2,2	147
	10%	11	1,2	21	2,2	119
	20%	11	1,2	21	2,2	104

Table 8.1: Dependability analysis results for extend storey design.

In the second case, the PJB-SJB cables, the detection units, the storeys and the optical modules are non-repairable. The SJBs are repaired one at a time with MTTR one month. In this case, the mean downtime (MDT) of a SJB is higher than the specified MTTR, so a conservative estimate of the MDT may be derived using queuing theory. Taking the unavailability of the SBJs to be equal to that of the other repairable components, the estimated SJB MTTF is around 11 years with MDT 1.2 months. The observed trend in the required MTTS for non-repairable components is similar to case 1. The MTTF values are lower than those of case 1, unless they exceed the 600yrs, because then the unavailability of non-repairable components becomes higher that the unavailability of repairable components assumed here.

In the third case, the PJB-SJB cables, the storeys and the optical modules are non-repairable. The SJBs and the detection units are repaired one at a time with MTTR one month: The MTTFs and MDTs for the SJBs are the same as in case 2. Taking the unavailability of the detection units to be equal to that of the other repairable components, the MTTFs and MDTs are 21 years and 2.2 months. The observed trend in the required MTTS for non-repairable components is similar to the previous cases. Since the MDT and the frequency of failure decreases the unavailability drops down, so lower MTTFs of the non-repairable components can be used. This benefit becomes more evident at low c and U_{max} values.

For larger unavailability of the DSI, the reliability requirements for the Detector Network components become more severe. For example, if the main electro-optical cable MTTF decreases to 2 years, the required MTTFs of the non-repairable components case 3, with c=20% and Umax=5%, increase to 490 years.

Results of the dependability analysis: redundancy of detector components

Assuming all detector network components have the same MTTF, the required MTTF to meet the system availability criterion is 375 years. If this MTTF is not technically achievable or too expensive the required extra unavailability can be provided by extra redundancy in the number of detection units and hence the OMs. If the achievable MTTF of the components is equal to 150 years then an additional 12% of OMs (1828) are required. If the technically achievable MTTF is 75 years then an additional 30% of OMs (4572) are required.

8.5 Failure mode and effect analyses

Once a component reliability requirement has been assessed (either as a design target or as a requirement stemming from the system reliability) it is necessary to determine whether the existing or the proposed design for this component can meet this requirement. A component reliability requirement is usually expressed in terms of its MTTF MTTFs (or other reliability measures, e.g. *Failure In Time* (FIT) rate) can be determined from manufacturer specifications or from in-house testing. The failure rates of complex systems are functions of the failure rates of the individual components that constitute the system. To determine this function a Failure Mode Effect and Criticality Analysis (FMECA) is performed [114,115]. An FMECA is a procedure for identifying potential failure modes in a system and classifying them according to their determined severity values.

A FMECA is usually carried out progressively in two parts:

- The first part identifies failure modes and their effects (Failure Mode and Effect Analyses [FMEA]).
- The second part ranks failure modes according to the combination of severity and the probability of that failure mode occurring (Criticality Analysis).

The FMEA (FMECA) procedure may be summarised as completing the following steps:

1. Define the system to be analysed;
2. Construct a hierarchical block diagram (e.g. RBD-reliability block diagram);
3. Identify failure modes at all levels;
4. Assign effects to the failure modes;
5. Assign severity categories to effects;
6. Enter other failure mode data;
7. Rank failure modes in terms of severity (and criticality);
8. Produce reports highlighting critical failures;
9. Feed results back to designers or maintenance planners;
10. Estimate the final system failure rate;

If failure modes are assumed catastrophic, i.e. where subsystem failure leads to system failure, steps 4 to 8 become redundant. In this case the analysis can be considered conservative. All the information is collected into a table similar to those used in defence applications (MIL-STD-1629A) or in the space industry (ECSS-Q-30-02A). The result of the FMECA becomes the input to the dependability analysis. To achieve a reliable dependability analysis for the neutrino telescope full FMECA analyses of the subsystems must be performed. These subsystems are optical module, electronic module, master module, backbone cable, interlink cable, secondary junction box, branch cable, primary junction box, main cable and shore electronics and power delivery. These subsystems are described in the product breakdown structures in chapter 3. The failure modes must include the power delivery, the slow control and the data acquisition. This will yield an availability estimate for the full telescope.
A fault tree analysis can then be used to optimize the availability of the full system. For instance, such an analysis on the storey architecture in the NEMO1 pilot project yielded the result that reliability is enhanced by limiting the number of components connected in series, reducing the number of external connectors and providing redundancy of protective systems.
The basic structure for these analyses is in place. The full analysis will, however, only be possible when final figures for failure rates are known. Many of these await prototype tests that will allow for more solid design specifications. The risk analysis will then aid the optimisation of the design and also provide input to the detector maintenance strategy. The design optimisation and maintenance strategy must necessarily also include results from physics performance studies and is also impacted by financial considerations. The final requirement specification for components will be a trade-off between performance, cost and reliability. The quality management system is in place to ensure the compliance of all components with the design specifications deduced from the above analyses.

8.6 Quality Control

The results from the quality assurance and from the dependability analysis show the need for qualification and optimization processes: reliability demonstration programs should be defined once reliability has been allocated to various components (e.g. using accelerating testing) in order to examine (and guarantee) the performance of the required function by the overall system. Such activity is reported in Figure 8-9. The reliability program is developed through a qualification process that implies a design review, a FMEA and dependability analysis, the design of proper tests to check the functions and requirements of components / systems are satisfied, the execution of the tests and the check of the results obtained that includes the FMEA and the dependability analysis. Once such process is concluded for all the components and systems of KM3NeT the quality control can be defined for all the processes of the project (i.e. suppliers' qualification, in factory test, acceptance test, transportation and packaging test, integration test, delivering test, pre-installation test, etc.). The FMEA and FTA will support the definition of the quality control.

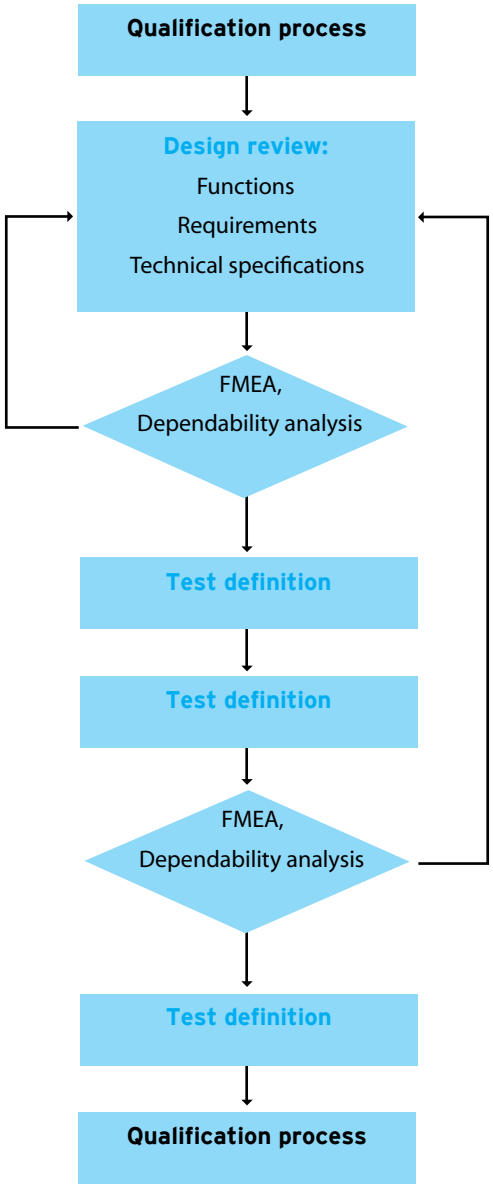

Figure 8-9: KM3NeT quality control process.

8.6.1 General rules for the quality control definition

A high level of reliability is required during the assembly processes, which can only be achieved by enforcing a rigorous quality control process at every stage of production.

For each type of item according to the ISO 9000 family, the QC activity will be adapted with respect to its specified level of dependability, its level of integration and its associated level of failure risk to the whole project. The QC would be done on a part or on entire item.

General rules

The general points for QC in assembly, transportation and test are the following one:

- **Resources**. To carry out this activity, at least, a dedicated and qualified quality supervisor will be identified for each production/assembly site. Operations shall be performed by trained and qualified personnel.
- **Documentation.** Dedicated documentation will be written, completed, recorded and archived following the Documentation Management Procedure.
- **Traceability.** Each product will be identified and stamped with a unique serial number, using an appropriate method such as bar codes. Using this serial number, each item will be traceable with respect to configuration, assembly and location details. These traceability records will be maintained and accessed via the QA database.
- **Non conformity.** The knowledge and traceability of defects is made through a Non Conformance Report (NCR). The NCR is initiated by people in assembly groups and then treated by the Local Quality Supervisor who releases it and follows the progress of the NCR.
- **Reviews.** Before each relevant phase, stage or operation, a review will take place to highlight all known risks.

Dedicated rules

The specific points in QA/QC for each type of activity are detailed below.

Assembly

The assembly process will be validated before starting production by a Production Readiness Review (PRR) and reviews with manufacturers. During production audits will be performed.

For each assembly activity (OM, container, DU…), a dedicated quality plan will be written. This document describes the process, the organization and the quality control to be applied.

As several sites will handle the same activities, a unique set of documentation for assembly and testing (procedures, test sheets…) will be defined and applied at all sites.

Each item or subsystem, delivered to an assembly site, will be accompanied by a conformity certificate of ensuring the item conforms to the defined specifications.

Logistics

The integrity of each item will be maintained and its location will be recorded during all logistical operations.

At each step, items will be accompanied by their "traveller" file (including its certificate of conformance and logbook).

Dedicated handling, storage, packaging and means of transport will be defined for each item, regarding its features/characteristics; operational conformity will be proved before transportation and checked after. Dedicated procedures will be written.

Test

For each test, a dedicated procedure will be written, identifying configuration, equipment, and protocols required. The results of each test will be recorded in the database. All equipment used during the testing procedure will itself have a file containing its maintenance and calibration schedules.

9. Cost and Feasibility of Construction

In this chapter, estimates of the capital investment required for the construction of the KM3NeT research infrastructure and of the running costs during its operation phase are described. In addition, a construction model is presented demonstrating that an installation time of below four years per building block is achievable with a reasonable deployment of human resources and assembly lines.

9.1 Capital Investment

The detection unit cost has been estimated using the following assumptions and procedures:

- With the exceptions quoted below, the costs of components were taken, in descending priority, from industrial quotations, corresponding costs as occurred in the pilot projects, public catalogues, and informal or confidential statements of providers.
- The costs of the photomultipliers are estimated according to informal and confidential statements of the corresponding companies.
- For the optical modules, the single-PMT option has been assumed for the flexible towers and the triangles, and the multi-PMT option for the slender strings.
- The costs for the junction boxes are based on the experience of the pilot projects.
- The on-shore installation is not included (except readout components).
- Contingency, cost for spares and inflation are not included. However, some of the prices include VAT of which an exemption can be expected in the governance framework of a European Research Infrastructure Consortium (ERIC).
- No costs of human resources for assembly are included; however, the sea operations needed for deployment are estimated based on the pilot project experience and include costs of crews, mobilisation and demobilisation of vessels.
- The design as described in this document has been assumed, i.e. no extra costs related to using fallback solutions have been included.
- A distance to shore of 100 km and a deep-sea network according to the "star option" of Section 3.4 has been assumed.

Based on the uncertainty of component prices, mostly caused by the fact that no binding quotations can be obtained at the current stage, the overall error margin on the total cost is estimated to be at least 20%.

The site dependence of the cost estimates is mostly related to the distance to shore (cable length and deployment) and to the water depth (even though the design is generally valid for all candidate sites, there are components and tools that need to be adapted to depths exceeding 4000m, such as connectors and ROVs). It is not expected that these issues will induce variations of more than 10% on the overall cost. The costs for the different design options are summarised in Table 9.1.

The goal of KM3NeT is to be the most sensitive neutrino telescope. Therefore it should surpass the performance of IceCube even at the declination where IceCube reaches its maximum sensitivity. Taking into account the above cost estimates, a detector with a total cost of about 220 M is required to achieve this goal. In Figure 9-1 the sensitivities are shown that can be obtained for such a cost with the different design options. It clearly indicates that a decision between the design options on the basis of a figure of merit "sensitivity per Euro" is inappropriate and that instead further technical tests and risk analyses have to be considered.

Concept	Cost per Detection Unit (k€)				No. of Detection Units in Simulation	No. of detection units for 220 M€ giving sensitivity of Figure 9-1
	Structure	Seafloor Infrastructure	Deployment	Total		
Flexible towers	535	70	87	692	127	320
Slender strings	254	42	40	336	310	650
Triangles	657	70	55	782	127	280

Table 9.1: Costs for constructing and deploying a detection unit for the different design concepts. For comparison the construction cost for the ANTARES experiment was roughly 20 M€ for 12 detection units. The number of detection units, used in the simulations of Chapter 6, is indicated. The sensitivity indicated in Figure 9-1 can be achieved for a cost of about 220 M€ and requires the number of detection units given in the last column.

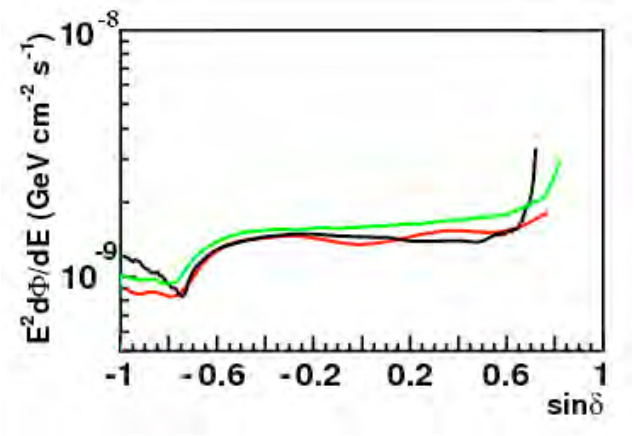

Figure 9-1 Sensitivity to point sources (E-2 flux) for one year of observation time, for a full detector of three configurations studied. See Section 6.3

9.2 Running costs

The running costs can be separated into three categories:

1. Maintenance of the detector

2. Power consumption of detector, shore station and data centre

3. Salary costs for shore station and data centre personnel

Category 2 and, for a given management structure (see below), category 3 are relatively straightforward to estimate but depend of course on the evolution of energy costs and salaries over the running period of the infrastructure. Category 1 depends on the maintenance plan of the detectors and therefore estimates require knowledge of the risks of failures inherent in the design and on the adherence to the quality assumed in the risk analysis. This implies that the error margins are larger in category 1 than they are in categories 2 and 3.

No running costs beyond the maintenance of the interface are currently taken into account for the earth and sea science installations.

9.3 Maintenance

The maintenance plan for the detection units will depend on their risk of failure. If the estimated failure rate of the detection units is at the level of 1% per year no maintenance will be necessary as the final 10-year failure rate is within requirements. A slightly increased detection unit failure rate of 2% per year, implying a 20% drop-out rate over 10 years, would require the manufacture of 10% spare detection units which can be immediately deployed. This is equivalent to a detector investment increase (or, at fixed budget, an average detector size decrease) of 10%. These options impact on the initial investment but do not contribute to long-term running costs. However, if the detection unit failure rate would be 10% or more per year, the full detector would have to be replaced in the running time of the experiment. This would clearly be unacceptable and would require a redesign. Therefore, a maximum detection unit failure rate of 5% is considered, and the maintenance costs estimated accordingly.

For the flexible tower structures, this would imply a repair rate of about 12 detection units per year, assumed to be performed in groups of 4. These costs are summarized in Table 9.2.

If a main electro-optical cable to shore fails, a separate operation for repair is necessary via MECMA. The experience with the repair of cables in pilot projects gives an estimate of 200 k€ for such an operation. Experience shows that there should be less than one repair every two years, providing a yearly maintenance cost of 100 k€. For junction box repairs that require ROV operations for connection and disconnection at most 500 k€ per year is assumed.

Action	**Cost in k€**
ROV operation for disconnection of 4 detection unit, together with reconnection of previous set of 4 detection units	150
Recovery sea operation	60
Redeployment	60
Replacement cost for failed equipment ~20% of unit cost	280
Total cost of repair of 4 detection units	550
Maximum total cost for repair per year (12 detection units)	1650

Table 9.2: Repair costs for one year assuming the repair of one detection unit per month.

Power consumption

The overall power consumption of the deep-sea detector will be 150 kW; for on-shore computers including cooling 350 kW are needed (assuming 1000 computers for shore station and data centre). This consumption adds up to 500 kW or about 4.5 GWh per year.
At the present price of 0.15€/kWh this gives a yearly power cost of 675 k€.

Human resources for shore station and data centre

Experience shows that a crew of 3 persons is adequate for local presence at a shore station. This crew will be required for computer, network and power maintenance. A presence at the shore station is also useful in terms of security. Including any overhead this corresponds to 100 k per person per year. For the running of the data centre around the clock, 3 persons for 3 shifts, i.e. a crew of 9 persons is required, corresponding to 9 times 150 k = 1650 k per year including overhead.

Project management

A professional project management, comprising a chief manager and a project office with 4 further employees (see Chapter 10) will require 200 k€ plus 4 times 120 k€ = 680 k€ of salaries per year, including overheads. Maintenance of the project office, consumables and related travel are estimated to cost 50 k€ per year.

Travel and subsistence of the members of the governing bodies in the ERIC (see Chapter 10) are assumed to cost 100 k€ per year.

Miscellaneous

- MECMA membership: 75 k€.
- Replacement of the 1000 computers after 5 years: 2000 k€/5 = 400 k€/year.
- Outreach activities: 100 k€ per year.

Total

The yearly total (see Table 9.3) thus varies between 2% and 2.5% of the investment cost. Normally the running costs of an experiment of this complexity and magnitude lies between 5 and 15% of the investment cost. The preliminary estimate indicates that KM3NeT will certainly remain at or below the bottom end of this range.

Cost item	Cost in k€ with ≤ 2% detection unit failure rate	Cost in k€ with 5% detection unit failure rate
Cable repair	100	
Junction box repair	500	
Power	675	
Human resources for shore station and data centre	1650	
Project management	830	
Miscellaneous	575	
Detection unit maintenance	0	1650
Total	4330	5980

Table 9.3: Estimate of the total maintenance cost for two maintenance policies.

10. Implementation

This chapter describes the planned path from the publication of this report to the KM3NeT construction and sketches the project structure during construction and operation. It presents the projected strategy for implementing Quality Control and finally a time line for the project.

10.1 Decision Path and Development Plan

The implementation of KM3NeT requires a series of decisions, based on technological and scientific evidence and taking into account political and funding aspects. In addition, engineering development is needed that feeds into decisions or is initiated by decisions. The basic questions to be addressed in this section are which decisions are to be taken, when and how.

Decision/Milestone	Input required
Verification of the deployment concepts for the mechanical options	Field tests with prototypes of each of the structures Risk analysis
Verification of the vertical backbone cables	Successful deployment and operation over several months; Risk analysis
Verification of the readout scheme	Laboratory tests; Simulation; Risk analysis
Verification and final engineering of the capsule OM concept	Lab prototype tests including long-term pressure test; Risk analysis
Site decision	Simulation and risk analysis; Cost analysis; Political convergence
Decision on mechanical structures and OMs	Results of the viability studies described above; Simulation results; Risk analysis; Refined cost analysis; Availability of components
Verfication of and decision on design of deep-sea power and data network	Site and mechanical design decision; Knowledge of detector size; Engineering design of junction boxes; Market analysis on availability and cost of components Risk analysis

Table 10.1: Technical steps towards the implementation of the KM3NeT infrastructure.

10.1.1 Decisions and Resources

In Table 10.1, the major technical and strategic decisions up to the stage where preproduction detection units can be constructed and the input needed for them are summarised. Overall, a materials budget of the order of 5M€, beyond the KM3NeT-PP resources is needed to arrive at the bottom line of the decision path. Some national funding is available. Further funding through national or regional channels has to be acquired, possibly with the support of an ASPERA common call. This may require the drafting of a Memorandum of Understanding between the parties involved. Aligning and coordinating this process will be a major task of the KM3NeT-PP.

It is planned that the construction of the KM3NeT neutrino telescope starts out with the construction of the shore station and the deployment of the main cable, part of the deep-sea network and ca. 10 preproduction detection units that have special provision for easy recovery and will allow for performing a high-statistics, *in situ* test of the complete design over about a year. In case of malfunctions the corresponding detection units will be recovered and analysed.

Any design flaws found will be mitigated in the mass production. If the preproduction detection units work well, they become part of the neutrino telescope. The resources for construction and deployment of this setup will be part of the KM3NeT construction budget.

10.1.2 Consortium Organisation

A set of activities and decisions are required for reaching the construction phase of KM3NeT. With the end of the Design Study in October 2009, the mandate of the corresponding decision-taking bodies has come to an end. Therefore, the Preparatory Phase project (KM3NeT-PP), running until the end of February 2012, plays a central role in providing a framework for establishing the governance structure required. It is assumed that at the end of KM3NeT-PP this governance structure will be in place and functional.

Altogether, the following two phases will occur:

1) The time between the end of the Design Study and the end of the KM3NeT-PP project. During this phase, the KM3NeT-PP decision bodies will monitor the process and steer the ongoing development. For activities not funded inside KM3NeT-PP, a Memorandum of Understanding (MoU) should be set up to regulate the distribution of tasks and responsibilities.

2) Following the KM3NeT-PP project, the final governance structure of the KM3NeT project will be in place in time to conclude contracts, issue tenders and generally allow KM3NeT to act as a legal entity.

10.1.3 Time lines

The decisions listed in Table 10.1 require the exact definition of the criteria along which they are taken. It is planned that these criteria are defined, agreed (see below) and documented by May 2010. All the following time scales have as a starting point this date.

For the viability decisions, extensive engineering work, repeated sea operations as well as the construction, deployment, operation and recovery of several engineering prototypes are necessary. It is expected that these activities will take 18 months. The site decision should, from a scientific and technical point of view, be taken as soon as possible in order to finalise design details. Also, the attractiveness for other countries and institutes to join the project will strongly increase once a site decision has been taken. However, this decision is also dependent on the process of political convergence towards project endorsement. The corresponding process is coordinated through the Preparatory Phase project. A decision must be taken after 18 months at the latest, to allow for a timely continuation of the project.

The final design will be presented in a detailed technical proposal, encompassing simulation and risk studies, using the site properties, as well as a refined cost estimate. The presentation of this document will coincide with the end of the KM3NeT-PP. At this stage it will be possible to launch KM3NeT construction. A period of 12-18 months is required to set up the assembly lines, to prepare tenders, to finalise the funding agreements. Thus, a start of production and installation is envisaged after 36-42 months, i.e. in 2013. This will start with the preproduction units mentioned above.

10.2 Future Project Structure

The KM3NeT Research Infrastructure will require an international governance structure allowing the stakeholders to establish a suitable legal entity, oversee the project, take financial and strategic decisions and execute the project management. The latter will be controlled by a body composed of representatives of the participating scientific institutions.

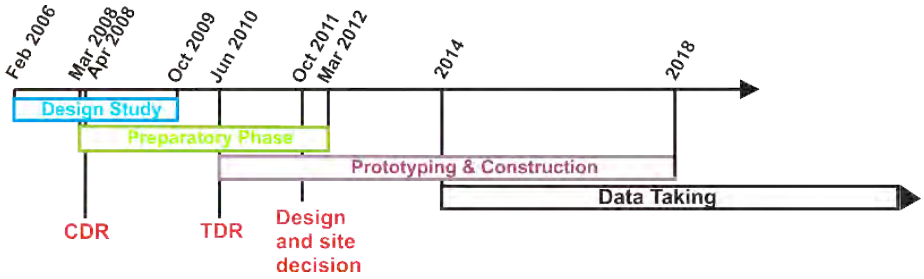

Figure 10-1: Overall time schedule of the KM3NeT project.

10.2.1 Governance

The exact definition of the legal and governance structure is a future task addressed by the Preparatory Phase project. The recently established *European Research Infrastructure Consortium (ERIC)*[7] is a candidate structure that is appropriate and has attractive and unique advantages: All requirements relating to the nature of the Research Infrastructure are fully satisfied by KM3NeT by virtue of the presence of KM3NeT on the ESFRI Roadmap;

The membership regulations of an ERIC are fully satisfied by KM3NeT;

The ERIC regulation also allows for the envisaged participation by countries outside the member states and associated countries. Furthermore, intergovernmental organisations can become ERIC members. This would allow, for example, for a future involvement of CERN.

For setting up an ERIC for KM3NeT, funding commitments and the site choice do not have to be fully established. It will, however, be necessary to endow the ERIC with an initial budget until the major funding commitments are decided. The initial statutory seat of the KM3NeT ERIC does not have to coincide with the country or one of the countries hosting the KM3NeT Infrastructure and may subsequently be changed. The establishment of a KM3NeT ERIC has some consequences and advantages. Subject to the member states' declaration recognising the KM3NeT ERIC as an international body the KM3NeT construction expenditure will not be subject to value added tax. In addition the KM3NeT ERIC could qualify for funding under title VI of the EC Financial Regulation as well for funding under the Cohesion Policy in conformity with the relevant Community legislation. The ERIC legal framework thus provides a sound basis for the future project structure. The prospects of setting up the KM3NeT ERIC will be explored in the KM3NeT-PP project.

10.2.2 Project Management

In the following, a management scenario is described that reflects the current plans of the KM3NeT Consortium. The precise management structure will be defined in the KM3NeT-PP project.

The core component will be a professional management team working on a full-time basis for the project. It will be led by the project manager, who directs a management team with competence in system engineering, quality control and risk management, legal and administrative issues, logistics and procurement. The management team will administer the construction and operation budgets. The project will be divided into subtasks addressed by appropriate working groups of experts. Examples for such subtasks are marine operations, assembly and construction, deep-sea technology, readout and electronics, physics and simulation, software. The convenors of the working groups will form the project coordination group which takes responsibility for the execution of the project and reports to the decision-making instance(s) established under the ERIC.

A data centre is planned for collection, mass storage, primary reconstruction and distribution of the neutrino telescope data and for providing the scientific community access to appropriate analysis tools. The administrative responsibility for the data centre is with the project manager.

[7] *Council Regulation (EC) 723/2009 (25 June 2009)*

11. Conclusions

A technical design has been presented for the KM3NeT Deep-Sea Research Infrastructure. The infrastructure will host a neutrino telescope with an instrumented volume of several cubic kilometres and provide the connectivity for an extensive multi-disciplinary earth and sea science observatory.

The neutrino telescope will detect neutrinos of cosmic origin by measuring the Cherenkov light induced by charged particles produced in neutrino interactions in the sea water or in the rock beneath the detector structure. This light is recorded in a three-dimensional array of light sensors located on structures with height of almost one kilometre and distributed over a base area of around six square kilometres. The installation will be located in the Mediterranean Sea at a depth of a few thousand metres and be permanently connected to shore for data collection.

The light sensors will be photomultiplier tubes housed in glass containers; the present design concept presents alternatives both for using large and small photomultipliers. These sensors are attached to vertical structures which are anchored to the seabed by a deadweight and held upright by a submerged buoy at the top. The deployment and behaviour of these "detection units" is a critical issue of the design and extensive field tests are required. As a consequence, alternatives are pursued, which yield the similar performance for the same cost. Final decisions will be made after the completion of prototype studies.

A readout technology has been developed that is suitable for all options considered. A sea-floor network of cables linking detection units to nodes of junction boxes will be installed for data transport and power provision. This network will also serve the earth and sea science observatory. On shore an installation for filtering and recording the incoming data is planned.

For the definition of the sensor layout in the sea, a detailed optimization has been performed based on the primary science objectives of the project. The resulting sensitivity for the detection of cosmic point-like neutrino-sources exceeds by a substantial factor that of the largest existing neutrino telescope, IceCube at the South Pole. For Galactic sources the sensitivity of KM3NeT surpasses that of the existing neutrinos telescopes, ANTARES in the Mediterranean Sea and Baikal in Siberia, by nearly two orders of magnitude.

Further essential considerations in the system optimization have been reliability and cost. The design study has shown that the major physics objectives can be met within a budget of 220 to 250 M€. The design is modular and so allows for staged implementation with continuously increasing science capabilities.

Final technical and site decisions will be made at the end of 2011 and a technical proposal will be presented in early 2012. Thereafter, the transition from ongoing prototyping activities to the construction phase will occur. Data taking will already start during the construction period with first science data becoming available around 2014.

Glossary

ADC	Analogue-to-digital converter
ADCP	Acoustic Doppler current profiler
AGN	Active galactic nucleus
AMANDA	Antarctic muon and neutrino detector array (neutrino telescope at the South Pole)
ANTARES	Astronomy with a neutrino telescope and abyss environmental research (neutrino telescope in the Mediterranean Sea)
ApPEC	Astroparticle physics European coordination
ASIC	Application specific integrated circuits
AUV	Autonomous underwater vehicle
CDM	Cold dark matter
CERN	Centre européenne pour la recherche nucléaire (particle physics laboratory)
CPU	Central processing unit
CTD	Conductivity-temperature-depth probe
CU	Crab unit (unit of flux for photons)
DEOS	Dynamics of Earth and ocean systems (deep-sea observatory network)
DAQ	Data acquisition
DB	Delta-Berenike
DMAS	Data management and archiving system
DMS	Data management system
DUMAND	Deep underwater muon and neutrino detector (neutrino telescope near Hawaii)
EBL	Extra-galactic background light
EDFA	Erbium doped fibre amplifier
EGRET	Energetic gamma-ray experiment telescope (satellite-borne)
EMSO	European multidisciplinary seafloor observatories (deep-sea observatory network)
ERDF	European regional development funds
ESFRI	European strategy forum on research infrastructures
ESONET	European seafloor observatory network of excellence
ESONIM	ESONET implementation model
EU	European Union
eV	Electron Volt
FPGA	Field-programmable gate array
FWHM	Full width at half maximum
GCN	Gamma-ray burst coordination network
GMES	Global monitoring for environment and security (monitoring network)
GOOS	Global ocean observing system
GPS	Global positioning system
GRB	Gamma-ray burst
GUI	Graphical user interface
GUT	Grand unified theories
GZK G	Greisen-Zatsepin-Kuzmin cut-off
H.E.S.S.	High energy stereoscopic system (TeV gamma-ray telescope)
ICG/NEAM	Intergovernmental Coordination Group for the Tsunami Early Warning and Mitigation System in the North East Atlantic, the Mediterranean and connected seas, part of IOC-UNESCO IOC – Intergovernmental Oceanographic Commission of UNESCO

IR	Infrared
LAERTIS	Laboratory in the abyss of Europe with real time data transfer to shore for interdisciplinary studies
LBNS	Long baseline acoustic navigation system
LED	Light-emitting diode
LIMS	Light intensity measuring system
MACRO	Monopole, astrophysics and cosmic ray observatory
MARS	Monterey accelerated research system (cabled observatory project)
MECMA	Mediterranean cable maintenance agreement
NEMO	Neutrino Mediterranean observatory (neutrino telescope in the Mediterranean Sea)
NEPTUNE	North east pacific time-integrated undersea networked experiments
NESTOR	Neutrino extended submarine telescope
OM	Optical module
ORFEUS	Observatories and research facilities for European seismology
pc	Parsec (astronomical unit of length)
PC	Personal computer
pe	photo-electron
PWN	Pulsar wind nebulae
QMS	Quality management system
RAM	Random access memory
RMS	Root mean square (deviation)
ROV	Remotely operated vehicle
RTV	Room temperature vulcanisation
SN	Supernova
SNR	Supernova remnant
spe	Single photon equivalent signal in a photomultiplier
SUSY	Supersymmetry
TDC	Time-to-digital converter
TDR	Technical design report
VHE	Very high energy
WIMP	Weakly interacting massive particle
X-HPD	Crystal scintillator hybrid photon detectors

Bibliography

[1] P.Kooijman *et al.* (ed.), *Conceptual design report for KM3NeT.* 2008, ISBN.9789064880315.

[2] R. Abbasi *et al.* (Ice-Cube collaboration), *Astrophys. J., 701(2009)L47.*

[3] F. Aharonian *et al., Rep. Prog. Phys.*, 71(2008)096901.

[4] F. Halzen, *Phys. Rept.*, 333(2000)349.

[5] P. Sapienza and G. Riccobene, *Riv. Nuovo Cim.*, 032(2010)591.

[6] T. Chiarusi and M. Spurio, *Eur. Phys. J.*, C65(2010)591.

[7] C. Spiering, *AIP Conf. Proc.*, 1085(2009)18.

[8] Dalhousie University. Ocean Tracking Network. http://oceantrackingnetwork.org/

[9] F. Briand, in *CIESM Workshop Monographs 34*, 2008.

[10] The Mediteranean Science Commission. http://www.ciesm.org/index.htm

[11] "EU Blue Paper on an Integrated Marine Policy," European Commission -- Marine Affairs COM(2007) 575, 2007.

[12] G. Bourlis *et al., Nucl. Instrum. and Meth.*, A602(2009)129.

[13] G. Bourlis *et al., Nucl. Instrum. and Meth.*, A626-627(2011)S163.

[14] A. Belias and A. Fotiou, *Nucl. Instrum. and Meth* , A626-627(2011)S176.

[15] B. Howe *et al., IEEE J. Oceans Eng*, 27(2002)267, http://www.neptune.washington.edu.

[16] M. Anghinolfi *et al., Nucl. Instr. Meth.* , A567(2006)527.

[17] Universal Joint Consortium. http://www.ujcosortium.com

[18] M. Ardid *et al., Nucl.Instr. and Meth.*, A602(2009)174.

[19] E. Migneco *et al., Nucl. Instr. and Meth* , A508(2008)111.

[20] D. Boersma, L. Gladstone, and A. Karle, in *Proc. of 31st Int. Cosmic Ray Conference*, Łódź, Poland,2009, contribution 1173; also arXiv:1002.4900 .

[21] A.G. Tsirigotis *et al., Nucl. Instrum. Meth.*, A595(2008)80.

[22] A. Leisos *et al., Nucl. Instrum. and Meth.*, A626-627(2011)S231.

[23] E. Anassontzis *et al., Nucl. Instrum. and Meth.*, A626-627(2011)S226.

[24] Ifremer. FP5 Assem project. http://ifremer.fr/assem

[25] T. Niedzielski, I.G. Priede, and A. Holford, *Marine Geophysical Researches*, 30(2009)217.

[26] KM3NeT, "Report on evaluation of existing water, oceanographic, biological and geological data from candidate sites," KM3NeT-WP5 summary http//www.roma1.infn.it/exp/nemo/KM3NeT/WP5_Deliverable5_1_090407.pdf , 2007.

[27] P. Amram *et al.* (ANTARES Collaboration), *Astroparticle Physics*, 19(2003)253.

[28] NEMO collaboration. (2002) nemoweb.lns.infn.it/sites/SiteReport/NEMO-Site-Report.pdf

[29] E. Trimonis and M. Rudenko, "Geomorphology and bottom sediments of the Pilos area," in Proc. of 2nd NESTOR International Workshop, Pylos, 1992, also at http://www.nestor.noa.gr/2nd/files/321_339_trimonis.pdf .

[30] E.G. Anassontzis *et al* , (NESTOR collaboration), NESTOR NOTE.160.2007, 2007.

[31] E. A. Widder, I. M. Latz, and J. F. Case, *Biol. Bull.*, 165(1983)791.

[32] P. J. Henning (ed.), *Bioluminescence in action*. London, U.K.: Academic Press, 1978.

[33] I. G. Priede *et al., Deep Sea Reseach, Part I* 55(2008)1474.

[34] J. Craig *et al., Nucl. Instrum. and Meth.*, A602(2009)224.

[35] J.A. Aguilar *et al.* (ANTARES collaboration), *Astroparticle Physics*, 23(2005)131.

[36] R. Riccobene *et al., Astroparticle Physics*, 27(2007)1.

[37] A. Capone *et al., Nucl. Instr. Meth.*, A487(2002)423.

[38] R. C. Baker and K. S. Smith, *Appl. Opt.*, 20(1981)177.

[39] E.G. Anassontzis *et al., Astroparticle Physics*, 34(2010)187.

[40] E.G. Anassontzis *et al.* (NESTOR collaboration), *Nucl. Instrum. and Meth* , A349(1994)242.

[41] P. Amram *et al.* (ANTARES Collaboration), *Astroparticle Physics*, 13(2000)127.

[42] J.A. Aguilar *et al.* (ANTARES Collaboration), *Astroparticle Physics*, 26(2006)314.

[43] M. Naumann-Godó, *Nucl. Phys.*, B (Proc. Suppl.) 172(2007)36.

[44] A. G. Tsirigotis, Ph.D.Thesis, Hellenic Open University, Patras, Greece, 2004.

[45] G. Aggouras *et al., Nucl.Phys.*, B(Proc. Suppl.)151(2006)279.

[46] T. Sjöstrand, *Comput. Phys. Commun.*, 82(1994)74.

[47] R. Engel *et al., Phys. Rev* , D80(2009)094003.

[48] S. Ando and J. Beacom, *Phys. Rev. Lett* , 95(2005)061103.

[49] V. Agrawal *et al., Phys. Rev.*, D53(1996)1314.

[50] E.V. Bugaev *et al., Phys. Rev.*, D58(1998)054001.

[51] A. Heijboer, Ph.D. Thesis, University of Amsterdam, Amsterdam, the Netherlands, 2004.

[52] D. Pandel, Diplom Thesis, HU Berlin, 1996.

[53] N. van Eijndhoven *et al., Astropararticle Physics*, 28(2007)456.

[54] J. Ahrens *et al., Nucl. Instr. Meth* , A524(2004)169.

[55] G.C. Hill *et al.*, "Statistical problems in particle physics, astrophysics and cosmology," in *World Scientific eProceedings*, 108.

[56] G. J. Feldman and R. Cousins, *Phys. Rev.*, D57(1998)3873.

[57] G.Ingelman *et al..*, Comput. *Phys. Commun.*, 101(1997)108134.

[58] P. Antonioli *et al., Astroparticle Physics*, (1997)357.

[59] G. Carminati *et al., Comput. Phys. Commun.*, 179(2008)915.

[60] C. Forti *et al., Phys. Rev.*, D42(1990)3668.

[61] Geant3. http://wwwinfo.cern.ch/asdoc/geant_html3/geantall.html

[62] C. Kopper, *Nucl. Instrum. Meth.*, A602(2009)107.

[63] A. Gazizov and M. Kowalski, *Comput. Phys. Commun.*, 172(2005)203.

[64] H. L. Lai *et al., Eur. Phys. J.*, C12(2000)375.

[65] D Heck *et al.*, Forschungszentrum Karlsruhe FZKA 6019, 1998.

[66] D. Chirkin and W. Rhode. http://icecube.wisc.edu/~dima/work/MUONPR/

[67] C. Kopper, Ph.D. Thesis, Univ. Erlangen, Erlangen, 2010.

[68] Geant4 consortium. http://wwwasd.web.cern.ch/wwwasd/geant4/geant4.html

[69] J. Carr *et al., in Proc. 30th Int. Cosmic Ray Conference*, Mérida, Mexico 5(2008)1413, and 5(2008)1417

[70] A. G. Tsirigotis, A. Leisos, and S. E. Tzamarias, *Nucl. Instrum. and Meth.*, A626-627(2011)S185.

[71] A. G. Tsirigotis, A. Leisos, and S. E. Tzamarias, *Nucl. Instrum. and Meth.*, A626-627(2011)S188.

[72] A. G. Tsirigotis and S. E. Tzamarias, *Nucl. Instrum. Meth* , A602(2009)91.

[73] C. D. Mobley, *Light and Water; Radiative Transfer in Natural Waters*. San Diego, U.S.A : Academic Press, 1994.

[74] A. Ivanoff, *Introduction à l'océanographie*. Paris, 1972, vol. 2.

[75] R. Coniglione *et al.*, in *Proc. of 31st Int. Cosmic Ray Conference*, Łódź, Poland, 2009, contribution 1358.

[76] A. Karle for the IceCube Collaboration, in *Proc. of 31st Int. Cosmic Ray Conference*, Łódź, 2009, Highlight Talk; also arX A.

[77] Kappes *et al., Astrophys. J.*, 665(2007)870.

[78] S. Basa *et al., Nucl. Instrum. Meth.*, A602(2009)275.

[79] P. Meszaros and M. J. Rees, *Astrophys. J.*, 405(1993)278.

[80] D. Guetta *et al., Astroparticle Physics*, 20(2004)429.

[81] R. U. Abbasi *et al.*, *Astrophys. J.*, 710(2010)346.
[82] E. Waxman and J. N. Bahcall, *Phys. Rev. Lett.*, 78(1997)2292.
[83] S. Razzaque *et al.*, *Phys. Rev.*, D69(2004)023001.
[84] M. Kowalski and A. Mohr, *Astroparticle Physics*, 27(2007)533.
[85] D. Dornic *et al.*, in *Proc. of 31st Int. Cosmic Ray Conference*, Łódź, Poland, 2009, contribution 55.
[86] A. Franckowiak *et al.*, in *Proc. of 31st Int. Cosmic Ray Conference*, Łódź, Poland, 2009, contribution 1173; also arXiv:0909.0631.
[87] R. Auer, *Nucl. Instrum. Meth.*, A602(2009)84.
[88] E. Waxman and J. N. Bahcall, *Phys. Rev.*, D59(1999)023002.
[89] A. Achterberg *et al.* (IceCube coll.), *Phys. Rev.*, D76(2007)042008, *erratum*, D77(2008),089904.
[90] M. Ackermann *et al.* (IceCube Coll.), *Astrophys. J*, 675(2008)1014.
[91] J. De Dios Zornoza, PhD. Thesis, Universitat de Valéncia, Valéncia, Spain, 2005.
[92] J. Ahrens *et al.* (IceCube collaboration), *Astroparticle Physics*, 20(2004)507.
[93] L. A. Anchordoqui *et al* , *Astroparticle Physics*, 29(2008)1.
[94] A.A. Abdo, *Astrophys. J. Letters*, 664(2007)L91.
[95] A.M. Taylor *et al.*, *Nucl. Instrum. Meth* , A602(2009)113.
[96] D. N. Spergel *et al* , *Astrophys. J. Suppl.*, 148(2003)175.
[97] P. Gondolo *et al* , *Journ. of Cosmology and Astroparticle Physics*, 0407(2004)8.
[98] F. E. Paige *et al.*,, *arXiv:hep-ph*, 0312045(2003).
[99] J. F. Navarro, C. S. Frenk, and S. D. M. White, *Astrophys. J.*, 490(1997)493508.
[100] S. Desai, *et al.*, *Phys. Rev.*, D70(2004)083523.
[101] G. Wikström, "A search for solar dark matter with the IceCube neutrino telescope," Ph.D. Thesis, Stockholm University, Stockholm, Sweden, 2009.
[102} R. Abbasi *et al.*, *Phys. Rev. Lett.*, 102(2009)201302.
[103] J. Braun, and D. Hubert (for the IceCube Collaboration), *in Proc. of 31st Int. Cosmic Ray Conference*, Łódź, Poland, 2009, contribution 834.
[104] J. L. Feng, K. T. Matchev, and T. Moroi, *Phys. Rev.*, D61(2000)075005.
[105] V. N. Lebedenko *et al.*, *Phys. Rev. Lett* , 103(2009)151302.
[106] J. Angle *et al.*, *Phys. Rev. Lett.*, 101(2008)091301.
[107] O. Behnke *et al.*, *Science*, 319(2008)933.
[108] D. Coronado, M. Acosta, and M. del Mar Cerb, *Economic Impact of the Container Traffic at the Port of Algeciras Bay*. Berlin: Springer, 2006.
[109] E. G. Jones *et al.*, *Marine Ecology Progress Series*, 251(2003)75.
[110] P. L. Tyack *et al* , *The Journal of Experimental Biology*, 209(2006)4238.
[111] R. S. Lampitt, *Nature*, 345(1990)805.
[112] M. Bĩlŷ, "Dependability of mechanical systems ," in *Studies in mechanical engineering 8*. Elsevier, 1989.
[113] I. A. Papazoglou and E. C. Marcoulaki, ""Dependability analisis of the conceptual design of a VLVNT in the Mediterranean Sea"," KM3NeT WD-KM3NeT-DS-T-RA-DA-09-001-REV0 1, 2009.
[114] "Procedures for performing a failure mode, effect and criticality analysis," AMSC N3074 (MIL-STD-1629), 1980.
[115] "Failure modes, effect and criticality analysis (FMECA)," ESA-ESTEC Requirements & Standards Division ECSS-Q-30-02A, 2001.
[116] E. Bernardini *et al.* (IceCube collaboration), *Nucl. Instrum. Meth.*, A567(2006)418.

Graphic design: ori ginale